AN ABSTRACT OF THE THESIS OF

Gopi K. Lingam for the degree of Master of Science in Industrial Engineering presented on September 20, 2010.

Title: Cooling Rate Limitations in the Diffusion Bonding of Large Microchannel Arrays

Abstract approved:

Brian K. Paul

A significant barrier to the diffusion bonding of large (i.e. 600 mm) microchannel devices is the large capital investment required to setup production. This large capital investment extends from long heating and cooling cycles leading to poor production capacities. Empirical studies in industry have shown that cooling rate is limited by the warpage of microchannel laminae which is believed to be caused by thermal buckling. In this thesis, the limits of cooling rates during the diffusion bonding of microchannel laminae were investigated. Findings confirm that cooling rates are limited by the thermal buckling of free-standing microchannel laminae during cooling of the device. Finite element analyses (FEA) of the transient thermal and static stress behaviors of

these microchannel laminae were conducted to identify the maximum cooling rates for different lamina thicknesses. FEA results were used to extrapolate implications for microchannel production.

©Copyright by Gopi K. Lingam

September 20, 2010

All Rights Reserved

Cooling Rate Limitations in the Diffusion Bonding of Large Microchannel Arrays

by

Gopi K. Lingam

A THESIS

submitted to

Oregon State University

in partial fulfillment of

the requirements for the

degree of

Master of Science

Presented September 20, 2010

Commencement June 2011

Master of Science thesis of Gopi K. Lingam presented on September 20, 2010.

APPROVED:

Major Professor, representing Industrial Engineering

Head of the School of Mechanical, Industrial and Manufacturing Engineering

---

Dean of the Graduate School

I understand that my thesis will become part of the permanent collection of Oregon State University libraries. My signature below authorizes release of my thesis to any reader upon request.

Gopi K. Lingam, Author

ACKNOWLEDGEMENTS

First of all I would like to deeply express my gratitude to my research advisor, Professor Brian K. Paul for his continual support, guidance and advice he gave me during my graduate study. I would like to specially thank Dr. Timothy Kennedy for being my minor professor in Mechanical Engineering and Dr. Karl Haapala for being on committee.

I would like to extend my appreciation to Dr. Jack Rundel for all his assistance in all my experimental work at the Microproducts Breakthrough Institute (MBI). My appreciation is extended to Mr. Steve Etringer for his valuable machining work and assistance in experimental work. I also like to express my appreciation to Keith Price for all his help in computer and software support.

I also like to thank all my fellow graduate students and friends for their encouragement, assistance and making my experience of studying abroad enjoyable.

Most of all, I would like to express my love and gratitude to my parents and siblings for their endless support in all aspects of my education both mentally and financially.

TABLE OF CONTENTS

Page

1. INTRODUCTION 1
2. LITERATURE REVIEW 5
2.1. Introduction 5
2.2. Scale-up of MPT devices 5
2.3. Microlamination 6
 2.3.1 Patterning and Registration 7
 2.3.2 Diffusion Bonding 8
2.4. Failures during Diffusion Bonding 9
 2.4.1 Creep 10
 2.4.2 Buckling 10
 2.4.3 Thermal Buckling 13
3. FINITE ELEMENT MODELING 18
3.1. Introduction 18
3.2. Case Study 19
3.3. Finite Element Analysis 20
 3.3.1 Uncoupled Heat Transfer Analysis 21
 3.3.2 Transient Stress/Deformation Analysis 24
3.4. Preliminary Results 26
4. EXPERIMENTAL APPROACH 33
4.1. Overview 33
4.2. Test Article Design and Material Selection 33
4.3. Test Article Fabrication 36
 4.3.1 Laser Machining 36

TABLE OF CONTENTS (Continued)

Page

4.3.2 Deburring 38
4.3.3 Flatness 39
4.3.4 Buckling Criteria 39
4.3.5 Flattening 41
4.3.6 Bonding 41
4.4. Load Cell Validation 42
4.5. Experimental Design 43
4.6. Thermocouple Set-up 44
4.7. Pressure Uniformity with Fuji Pre-scale Film 47
4.8. Diffusion Bonding Cycle 49
5. RESULTS AND DISCUSSION 52
5.1. Critical Buckling Stresses 52
5.2. Finite Element Analysis Results 53
5.3. Experimental Results 55
5.4. Discussion 57
5.5. Sensitivity Analysis 60
6. CONCLUSIONS 62

LIST OF FIGURES

Figure Page

1-1. *Classification of microfluidic devices (Pluess 2004)* 2

2-1. *Scale-up of microchannels by numbering-up channels, layers and devices.* 6

2-2. *Schematic of microlamination approach* 7

2-3. *Geometry of (a) uniform flow channels, (b) non-uniform flow channels (fin buckling) [40]* 16

2-4. *Metallographic images of a microchannel device bonded using (a) internal convective heating; and (b) vacuum hot press [7]* 17

3-1. *Exploded view of the stainless steel test article used used ICH and VHP processes [33]* 20

3-2. *Stack meshed with hexagonal mesh elements* 22

3-3. *Actual diffusion bonding cycle times of the sample [7]* 24

3-4. *Thermocouple data recorded for the first minute of cooling cycle [15]* 28

3-5. *Temperature profiles of the center and surface of the fin in the first minute of cooling cycle [15]* 28

3-6. *Temperature distribution across the shim at an instant in the first minute of cooling cycle (thermocouple assumed to be on periphery of graphite block)[15]* 29

3-7. *Stress distribution across the fin at the instant of highest thermal gradient (thermocouple assumed to be on periphery of graphite platen)[15]* 30

3-8. *Stress plot of a node at the point of maximum compressive stress in the middle shim (thermocouple assumed to be on periphery of the graphite block) [15]* 30

3-9. *Temperature distribution across the middle shim at an instant in the cooling cycle (thermocouple assumed to be half inch from edge of graphite platen)* 32

3-10. *Stress distribution across the middle shim at an instant in the cooling cycle (thermocouple assumed to be half inch from edge of graphite platen)* 32

4-1. *Test article used in this study with channel and fin areas* 35

4-2. *Warpage in lamina after patterning features on the laser using (a) non-optimized parameters, (b) optimized parameters* 37

4-3. *Scan locations on the test articles for laser burr* 38

4-4. *Profiler images of laser burrs (a) before and (b) after flattening cycle* 39

4-5. *Relation between hot press GUI readout and load cell reading* 43

LIST OF FIGURES (Continued)

Figure | Page

4-6. *(a)Location of thermocouples in the vacuum chamber (b) Vacuum port in which thermocouples are connected to thermocouple elements* 46

4-7. *Locations of thermocouples in the ceramic block*.. 46

4-8. *Thermal data logger graphs showing the actual cooling rates of the stack during diffusion bonding cycles*.. 47

4-9. *Pressure distribution of the platens measured using sensitive films before machining*.. 48

4-10. *Pressure distribution of the platens measured using sensitive films* 48

4-11. *Pressure distribution of the platens with ZYP coating* 49

5-1. *Temperature and stress profiles for a lamina thickness of 100 µm cooled at a rate of 3.5 °C/min* 53

5-2. *(a) Temperature distribution and (b) stress distribution in 100µm shim, run at a cooling rate of 5 °C/min*.. 55

5-3. *Experimental runs showing buckled and non-buckled lamina thickness with respect to cooling rate* 56

5-4. *Comparison of FEA predicted cooling rates where thermal stresses equal to critical buckling stress* 57

5-5. *Profiler scan over a length of 15mm on the fin of thickness 100µm cooled at a rate of 3.5 °C/min*.. 58

5-6. *Profiler scan over a length of 15mm on the fin of thickness 100µm cooled at a rate of 5 °C/min*... 59

5-7. *Cooling rates comparison for different fin spans 61*

LIST OF TABLES

Table Page

4-1. *Mechanical properties of copper alloy 110 at room and bonding temperatures* . 36

4-2. *Laser parameters used to pattern features on the copper laminae* 37

4-3. *Cooling rates at which the experiments were conducted*...................................... 43

5-1. *Critical buckling stresses for fin buckling with respect to thickness* ……………..52

LIST OF APPENDICES

Appendix A: Test Article Drawings ……………………………………………………69

Appendix B: FE-Model Simulation Settings ……………………………………………72

Appendix C: Properties of Materials at Bonding Temperature ……………………75

Appendix D: FE-Model Results ……………………………………………………76

DEDICATION

Dedicated to my beloved grandfather

Krishna Murthy Lingam,

1930 – 2003

COOLING RATE LIMITATIONS IN THE DIFFUSION BONDING OF LARGE MICROCHANNEL ARRAYS

CHAPTER 1

1. INTRODUCTION

In recent years, there has been a growing interest in the field of microfluidics. Microfluidics deals with the behavior and manipulation of fluids within sub-millimeter scale channels (i.e., microchannels). Microfluidic devices can mainly be classified into two groups: analytical devices, mainly referred to as micro total analysis systems (μ-TAS), and arrayed devices, referred to as micro energy and chemical systems (MECS) or microchannel process technology (MPT). These two major categories have significant differences in their function and in the materials and fabrication technologies needed to produce them. Micro total analysis systems are used to generate information from nano and micro-liters of fluids. MPT devices are designed to process bulk quantities of fluids through the use of microchannel arrays.

MPT devices are microfluidic systems with embedded arrays of microchannels for processing high rates of fluid mass and thermal energy. Microchannels provide increased surface-to-volume ratios leading to accelerated heat and mass transfer compared to conventional macro-scale tubes [19]. For diffusion limited processes, MPT devices are capable of reducing the sizes of fluidic systems by a factor of 5 to 1000 leading to mass and energy applications characterized by their need for mobility and

compactness. MPT applications include advanced climate control [28], solvent preparation [13], micro-combustion [14] and fuel processing [3] among many others.

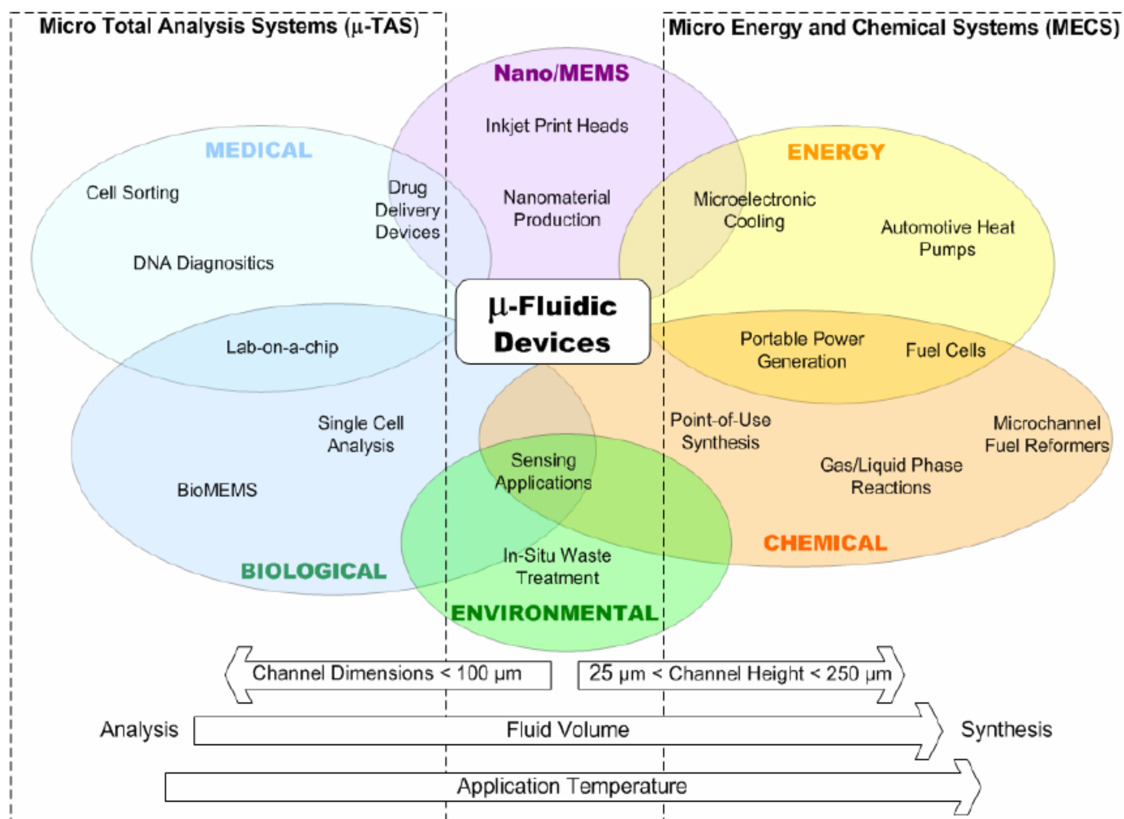

Figure 1-1. *Classification of microfluidic devices (Pluess 2004)*

The vast majority of μ-TAS devices involve the use of silicon, glass and polymers which make electromechanical integration easier [16][24]. However, the functionality of MPT devices demands the physical, chemical, thermal and mechanical properties of more traditional engineering materials including metals, polymers and ceramics. Further, the

sizes of MPT devices dictate the use of more economical materials than single crystal silicon.

Mostly, MPT devices are produced using microlamination architectures [4][38]. Microlamination architectures involve the patterning, registration and bonding of thin metal or polymer sheet (or laminae) to produce a single monolithic structure with embedded microchannels. Laminae patterning can include photochemical machining (PCM), laser machining, wire electrodischarge (wire EDM) or stamping processes. Registration step employs pinhole or edge registration techniques. Diffusion bonding, diffusion brazing and other forms of brazing are typically used to bond the registered laminae into a single device [34].

For diffusion bonding, laminae are typically heated to the bonding temperature and then an appropriate bonding pressure is applied. The laminae stack is held at these conditions for a certain period of time (dwell time) so that solid state diffusion occurs across faying surfaces of the metals and forms a monolithic device. The bonding pressure must be uniformly distributed throughout the device in order to prevent poor bonding conditions leading to fluid leakage or warpage. In diffusion bonding or diffusion brazing, it is well known that cycle times are often dictated by the heating and cooling rates used during the process. It is also widely believed that heating and cooling rates, that are rapid, can generate thermal gradients and corresponding thermal stresses across the device leading to thermal buckling of fins adjacent to microchannels.

This research investigates the thermal stresses that arise in the microchannel fins due to cooling rates. Cooling rate and fin thickness are examined to conclude if thermal buckling of microchannel fins is a concern and, if so, what constraints are required on cooling rates.

Chapter 2 summarizes the technical literature about fabricating MPT devices and different failure modes observed in the past during their fabrication. Chapter 3 presents the finite element modeling (FEM) approach used for analyzing the cooling cycle of a laminae stack during diffusion bonding. Chapter 4 explains the experimental approach used to validate the results of the FEM. A comparison of the FEM and experimental results is summarized in chapter 5. Chapter 6 states the conclusions of the study and future work that can be done in this area.

CHAPTER 2

2. LITERATURE REVIEW

2.1. Introduction

Distributed MPT systems are expected to be produced in high volumes at relatively low cost similar to that of integrated circuits (IC) and micro electro mechanical systems (MEMS) industries. IC and MEMS manufacturing is mainly based on silicon, on which sub-micrometer features are implemented. However, typical dimensions of microchannels in MPT devices are in the range of 25 to 500 μm.

2.2. Scale-up of MPT devices

Practical applications of MPT devices involve the processing of bulk fluids and thermal energy management. The large volumes of fluid processed in MPT devices require the arraying of microchannels. The process of scaling-up microchannel devices is referred to as “numbering-up” since increasing fluid volumes are managed by increasing the number of channels. Arrays of microchannels are patterned across a single lamina and many such laminae are then stacked and bonded together to form a two-dimensional array of channels. These arrays can be banked together to further increase the volume of fluid processed (Figure 2-1).

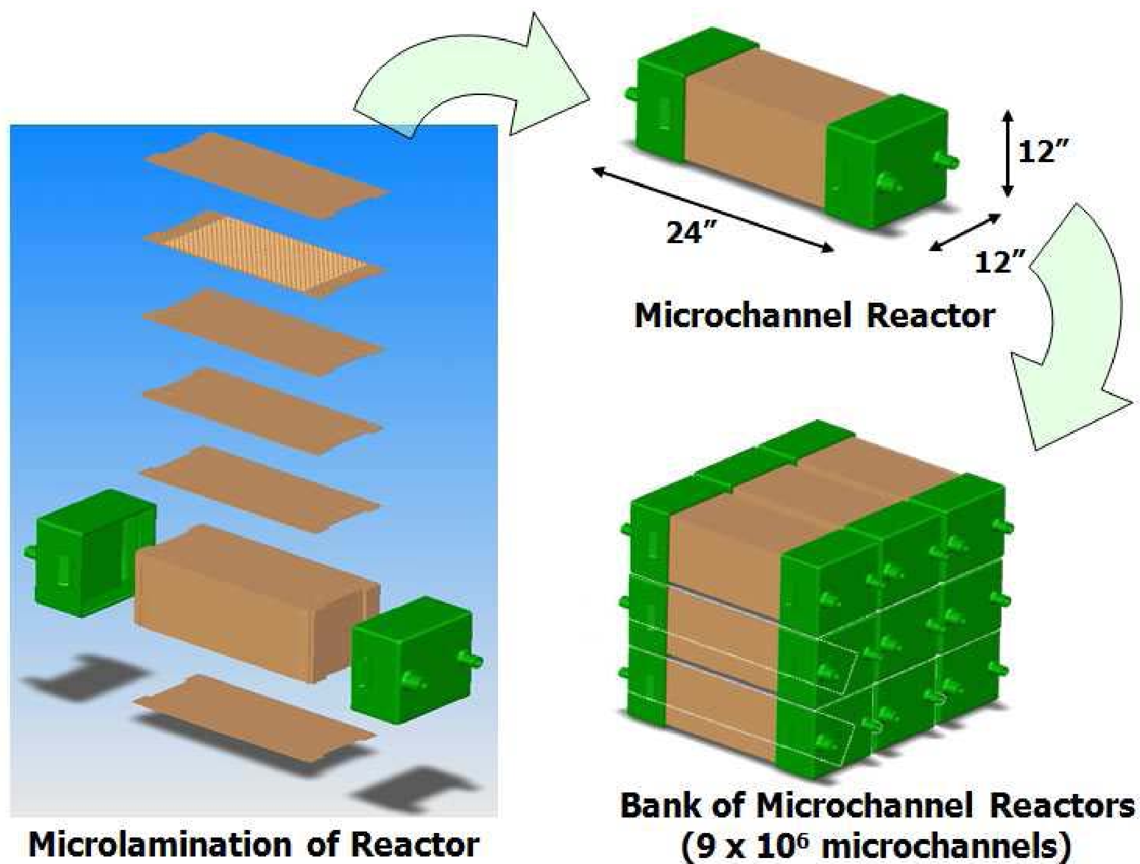

Figure 2-1. *Scale-up of microchannels by numbering-up channels, layers and devices.*

2.3. Microlamination

The majority of MPT devices are produced using microlamination architectures [14] [36][37][27]. Microlamination is a fabrication protocol for producing monolithic MPT devices with embedded geometries and flow patterns [19][4] necessary for the microchannel processing of bulk fluid volumes. In general, microlamination architectures consist of three major steps: (1) patterning, (2) registration and (3) bonding. Figure 2-2

shows an exploded view of a typical microchannel array design used for heat and mass transfer.

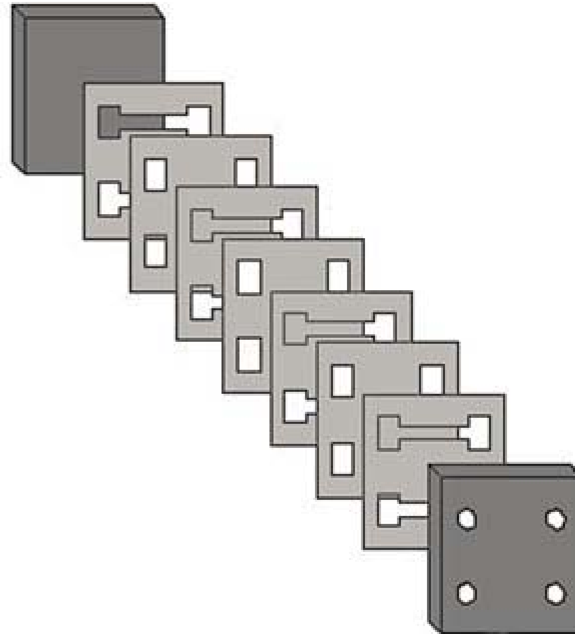

Figure 2-2. *Schematic of microlamination approach*

2.3.1 Patterning and Registration

Patterning is the process of making micro features on thin sheets (laminae). Various techniques have been employed for patterning of individual laminae. Patterned laminae with complex channel features and good resolution are typically produced using photochemical machining (PCM), laser machining, wire electrodischarge (wire-EDM) or stamping. Wire-EDM can be employed to cut a stack of hundreds of laminae at the same

time. Stamping is a potential low cost alternative for mass production. Laser machining is used when micro-features are to be patterned on polymers. After patterning, the laminae can be aligned, or registered, using pins and precise pinholes [32]. A thermally-enhanced edge registration (TEER) technique [40] has been used to align laminae. The TEER technique employs the difference in thermal expansion between fixtures and laminae to precisely register the laminae during high temperature bonding cycles.

2.3.2 Diffusion Bonding

Diffusion bonding, diffusion brazing, brazing and other forms of bonding have been used to bond registered laminae into a monolith device [34]. Diffusion bonding is mainly influenced by three major parameters: (1) bonding temperature, (2) bonding pressure and (3) bonding time. Diffusion bonding is typically done in a vacuum hot press (VHP) where the sample is heated to the bonding temperature in vacuum by radiation from the heating element onto the surface of the lamina assembly followed by intra-assembly conduction. Once at the bonding temperature, laminae are pressed uniformly for a specific period of time necessary for solid state diffusion to take place across lamina boundaries. The bonding temperature reduces the yield stress of materials and activates diffusion and mobility of atoms in the lattice, whereas the bonding pressure increases contact between faying surfaces by plastically deforming surface asperities. A surface finish of 0.4 μm R_a or better is typically necessary to achieve bond strength close to that

of the parent material [32]. The bonding of materials typically takes place at between 0.5 and 0.7 of the melting temperature of the lowest melting material. Typical bonding pressures range from 5 and 10 MPa for carbon steels, 7 and 12 MPa for stainless steels and 3 and 7 MPa for aluminum alloys [32]. Bonding time is typically over several hours depending on the applied temperature and pressure. The strength of the resultant bond is proportional to the square root of the bonding time. For a properly diffusion bonded structure with minimal voids and inclusions on the bond line, the bond strength ideally would be the same as that of the parent material.

2.4. Failures during Diffusion Bonding

Prior studies have shown that the diffusion bonding step can be critical for controlling yield in microlamination processes where improper bonding conditions can lead to leakage or warpage defects and flow maldistribution problems across microchannel arrays. Paul et al. [6] successfully analyzed the design limits on aspect ratios in counter-flow microchannel arrays and results were matched with empirical data. Findings showed that leakage due to poor bonding conditions were predicted in regions of test articles where the stress distribution approached the tensile/compressive boundary. Schubert, et al. [23] noted that the lack of structural support in microchannel designs could result in the collapse of microchannels during operation. Warpage is less likely to

occur in small test articles where spans are small. In larger devices, complex header structures can lead to large unsupported spans.

Two common warpage mechanisms within MPT devices generated during the diffusion bonding process are creep and buckling described below.

2.4.1 Creep

Application of bonding pressures over long durations can result in warpage of microchannel structures due to creep. Creep is the permanent deformation of a material at stresses below the yield strength of the material. Creep is a time, temperature and pressure phenomena. Higher temperatures reduce the amount of time for which pressure has to be applied on the material for creep to occur. Typically, creep causes fin warpage by causing adjacent fin supports to deform in a non-uniform manner.

2.4.2 Buckling

Buckling is a failure mechanism characterized by the sudden collapse of a structural member due to lateral deflection when subjected to high compressive stresses. The actual compressive stress at the point of buckling can be less than the yield compressive stress that the material is capable of withstanding. This mode of failure can

also be described as failure due to elastic instability. Buckling of microchannel fins during diffusion bonding has been found to be caused by several factors including differential thermal expansion between laminae and bonding fixtures [40] and Poisson's ratio [9].

In 1757, Leonhard Euler derived a formula for the maximum axial load that a slender, ideal column can carry without buckling (Equation 1). The critical buckling load causes the column to be in the state of unstable equilibrium. Any increase of load in the axial (longitudinal) direction or application of slight force in the lateral direction will cause the column to buckle.

$$F_{critical} = K\,\frac{\pi^2 EI}{(b)^2} \qquad \text{(Equation – 1)}$$

where,

$F_{critical}$ = Critical buckling force [N]

E = Young's modulus of the material [Pa]

I = area moment of inertia [m^4]

b = unsupported structure span [m]

K = column effective length factor

Alfutov [26] has done additional work based on Euler's formula and developed additional formulas. In order to adapt the formulas for microchannel applications, discussed in previous sections, critical buckling load for rectangular plates was implemented. The microchannel plate structure (subjected to buckling) is supported along

two edges and has the other two edges free. Considering the length as *l* and span as *b*, critical buckling stress can be determined as:

$$\sigma_{critical} = K\,\frac{\pi^2 D}{(b)^2} \qquad \text{(Equation – 2)}$$

where

D = bending stiffness / moment parameter of the plate [Pa.m]

The bending stiffness parameter for a plate relates the applied bending moment to the resulting deflection. It is the product of elastic modulus (E) and area moment of inertia (I) which is represented as

$$D = \frac{Et^3}{12(1-\vartheta^2)} \qquad \text{(Equation – 3)}$$

where

t = plate thickness [m]

Applying the above equations and assuming that both sides of the plate are fixed, (which are bonded in our case) critical compressive / buckling stress for a plate structure can be written as:

$$\sigma_{critical} = \frac{\pi^2 E}{3(1-\vartheta^2)}\left(\frac{t}{b}\right)^2 \qquad \text{(Equation – 4)}$$

It can be noted from the above formula that the length factor *l* of the microchannel has been cancelled out and thus has no effect on the model. The formula relates compressive

stresses to the material's mechanical properties (*E* and ν) and the structural dimensions (*t* and *b*).

2.4.3 Thermal Buckling

When a structural element is subjected to a temperature gradient due to a cooling effect on one end, the material will contract in different amounts in accordance with its coefficient of thermal expansion (CTE) and the temperature distribution. If the resultant thermal strain produces compressive stresses beyond the critical buckling stress of the structural element, the element will buckle. This phenomenon is known as thermal buckling. Four major scenarios that induce thermal stresses within a material are:

i. When a body is non-uniformly heated. If different portions of a body are exposed to different thermal conditions, the hotter portion of the body tries to expand more in comparison to the colder portion. Expansion of the hotter portion is restricted by the colder portion thus inducing thermal strains within the body.

ii. A CTE mismatch. If a layered composite is exposed to a uniform temperature change, individual materials expand according to their CTE. One metal expands or contracts more compared to the other. If the interfacial bond between the materials holds, one material imposes constraints on the other.

Layered composite of 2 materials,

CTEs: $\alpha 1 > \alpha 2$

Composite with materials of different CTE's

Initial and final temperatures: T_i and T_f

Stress in material1: $\sigma 1 = E1(\alpha 2 - \alpha 1)\Delta T$

Stress in material2: $\sigma 2 = E2(\alpha 1 - \alpha 1)\Delta T$

where,

E is the Young's modulus of the material and

ΔT is the raise in temperature from initial state to final state

iii. CTE anisotropy. For some materials, the CTE can differ along different crystal directions. Changes in temperature across the material results in regions of expansion/compression in different directions. On cooling of these materials, stresses develop at grain boundaries which may result in microcracks.

iv. Uniformly heated and restrained. A body free of any forces and restraints is subjected to temperature change uniformly from an initial temperature T_i to a final temperature T_f. Stresses do not arise within the body because the expansion/contraction is unrestrained. The only case where a body which is uniformly heated results in thermal stresses is when it is restrained either in translational or rotational motion.

A recent study at Oregon State University showed that the diffusion bonding cycle time can be the largest of all cost factors in the production of MPT devices, representing 40 to 87% of the fabrication cost [33]. In diffusion bonding, cycle times are often dictated by the heating and cooling rates used during the process. It is widely

believed that these heating and cooling rates can generate thermal gradients within unsupported microchannel fins leading to thermal buckling. This fin deformation or warpage, shown in Figure 2-3, can lead to flow maldistribution and poor device performance. Due to these considerations, cooling rates are typically limited to 5°C/min for small devices (< 25mm) and as low as 0.1°C/min for large ones (> 500mm).

In order to increase heating and cooling rates and thus reduce cycle times, an internal convective heating (ICH) technique was recently developed by Paul and Bose [7]. This technique utilizes the existing internal flow channels inherent in microchannel devices to rapidly heat or cool the device from the inside out, thereby permitting faster heating and cooling cycles. In prior work, a comparative study was done between microchannel structures bonded using VHP and ICH approaches [7]. It was found that under identical bonding conditions i.e., (time for which bonding pressure was applied, environment and surface conditions) the channels bonded using the VHP were more deformed compared to those bonded using the ICH method (Figure 2-4). The mean channel warpage in the VHP sample was 15.5% with a standard deviation of 1.5%, whereas the mean channel warpage in the ICH sample was 0.7% with a standard deviation of 0.7%. It is assumed that this was because the thermal gradient within the device bonded in the VHP was greater than that bonded using the ICH method suggesting thermal buckling.

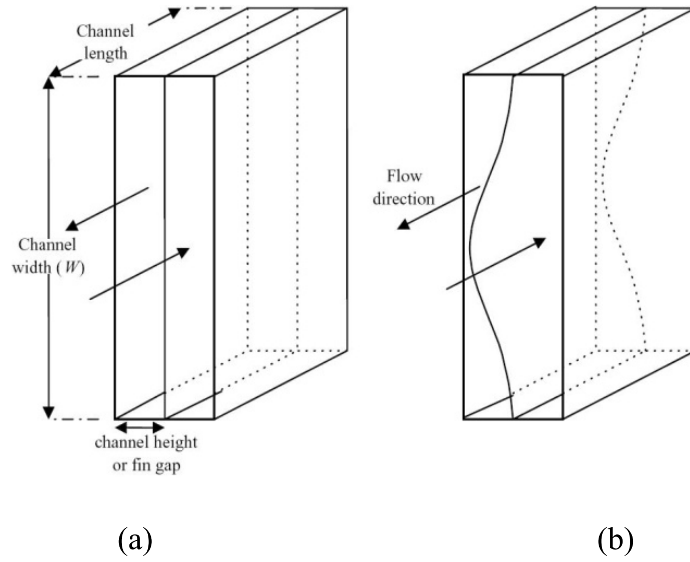

Figure 2-3. *Geometry of (a) uniform flow channels, (b) non-uniform flow channels (fin buckling) [40]*

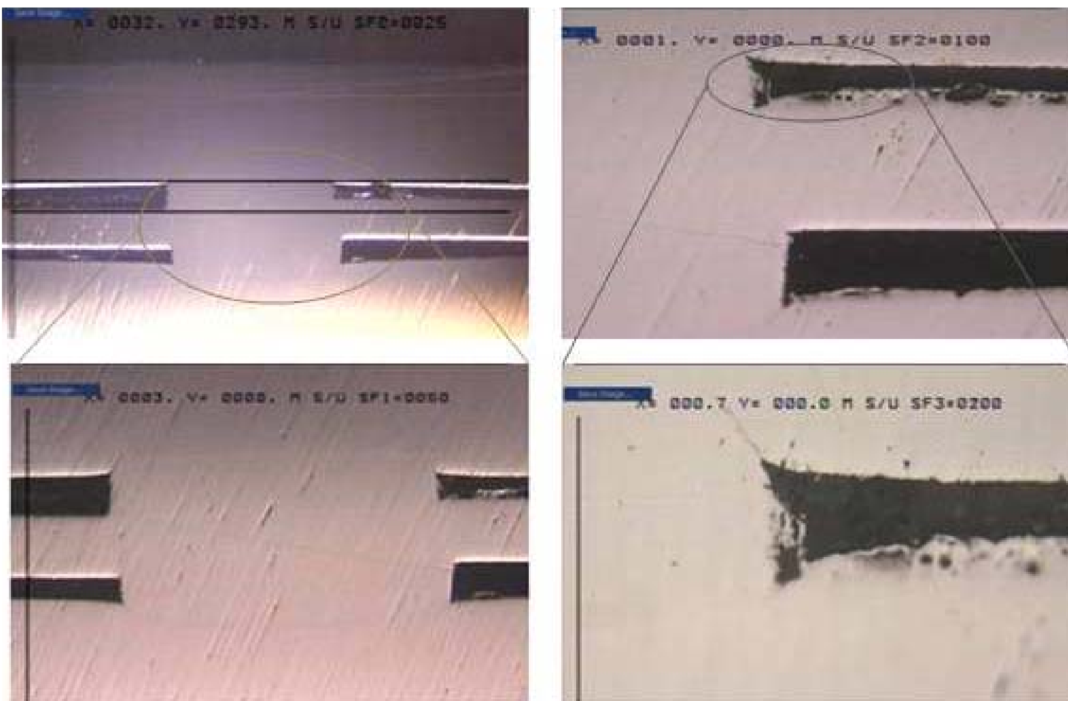

(a)

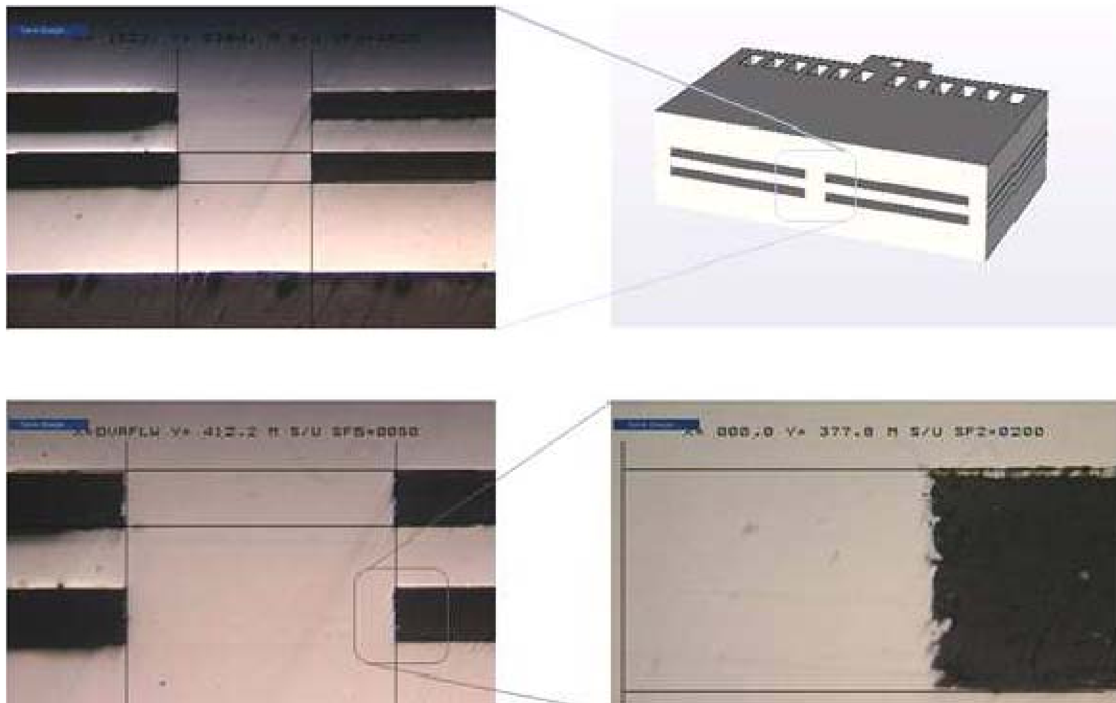

(b)

Figure 2-4. *Metallographic images of a microchannel device bonded using (a) internal convective heating; and (b) vacuum hot press [7]*

Other studies have reported conditions for thermal buckling in plates. Jones 0[30] studied the plastic thermal buckling of uniformly heated bars and plates with temperature dependent material properties. Gossard et al., [25] analyzed the mechanism of plate buckling due to spatial thermal gradients, which inspired further experiments on thermal buckling [34][15]. Rizk and Radwan [2] studied the breaking of a plate, of finite thickness and with an edge crack, due to sudden thermal transient stresses. These studies have given ground to analytically estimate the compressive stresses required for a plate to buckle. These analytically computed values are used in this thesis to develop the FE model descried in the next chapter.

CHAPTER 3

3. FINITE ELEMENT MODELING

3.1. Introduction

Finite element analysis (FEA) software has been used to simulate the mechanical behavior of microchannel structures under operating conditions. Zhou et al. [18] used FEA software to analyze the visco-elastic deflection and stresses of microchannel structures when subjected to internal (operating) pressure. In this manner, FEA can facilitate a better understanding of design limitations of arrayed microchannel components during operation.

Further, finite element analyses (FEA) have been employed in the past to understand the stress states within bonded joints and laminated stacks during bonding. Travessa [12] employed FEA to evaluate residual stresses in joining aluminum oxide and stainless steel using an interlayer. Similarly, finite element simulations were conducted by Feng [20] to estimate the thermal stresses generated during diffusion bonding of Al_2O_3 ceramic to aluminum. More recently, Paul et al. [6] employed the FEA technique to analyze stress state between laminae during diffusion bonding to determine the conditions necessary for diffusion bonding to take place in areas not subjected to direct bonding pressure. Pluess and Paul [10] used FEA to model the resultant bonding pressure generated by a diffusion bonding fixture based on differential thermal expansion.

In this thesis, a finite element model is developed to predict the cooling rates under which thermal buckling will happen in microchannel fins of MPT devices during diffusion bonding. The model is subjected to uncoupled thermal-mechanical analysis with linear elements in ABAQUS.

3.2. Case Study

To investigate the use of FEA to model the thermal buckling behavior discussed above, experimental results from earlier work performed by Paul and Bose [33] were used. Paul et al. [7] developed a novel approach known as internal convective heating (ICH) process to increase the heating and cooling rates of diffusion bonding cycle. This technique utilizes the existing internal flow channels inherent in the microchannel devices to rapidly heat or cool the device from inside out, thereby reducing the diffusion bonding cycle time considerably. A comparative study was made between the ICH approach and that of a conventional heating process performed in a vacuum hot press (VHP). It was found that under identical bonding conditions, the microchannel devices bonded in a VHP had highly deformed channels compared to those bonded using the ICH process. It was expected that the warpage found was due to thermal buckling of fins within the device, as the diffusional distance for heat transfer in VHP was more than 10 times that in the ICH process.

Figure 2-4 shows metallographic images of the stainless steel microchannel device bonded using ICH process and in VHP. An exploded view of the solid model of

the device for better understanding is shown in Figure 3-1. The assembly consists of a middle lamina and four flow laminae, two on either side of the middle lamina. The middle lamina which has the dimensions of 25 mm x 25 mm x 0.381 mm was considered for studying the buckling behavior due to thermal compressive stresses. The FEA model includes graphite platens (blocks) of dimensions 50mm x 50mm x 25 mm on either side of the assembly.

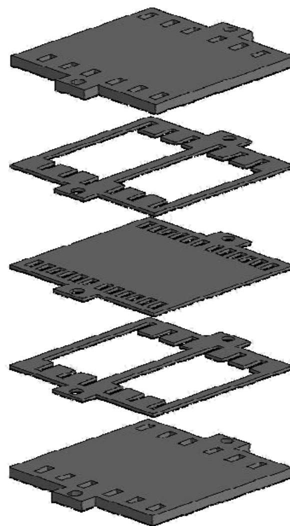

Figure 3-1. *Exploded view of the stainless steel test article used used ICH and VHP processes [33]*

3.3. Finite Element Analysis

An ABAQUS model was developed to represent the conditions of the interior of a vacuum hot press (VHP). In most cases, diffusion bonding of a laminae stack is done in a hydraulic VHP. In the present study, the VHP included a cylindrical heating chamber of 75 mm internal diameter x 150 mm high. Graphite hydraulic rams of 50 mm diameter

were present at the center of the chamber and employed to hold and apply pressure on the lamina stack. Heating elements and coolant circulation tubes were present in a shell surrounding the chamber. Heat was transferred from the heating elements in the shell to the surface of the laminae stack by radiation and from the surface to the inside of the laminae by conduction.

A two-step, sequentially-coupled thermal-stress analysis was performed in ABAQUS. The most common type of sequentially coupled thermal-stress analysis is one in which the temperature field in the model does not depend on the stress field but the stress field is dependent on temperature field. In the present case, the analysis was performed by first conducting an uncoupled heat transfer analysis to generate a temperature distribution followed by a stress/deformation analysis based on the results from the heat transfer analysis.

3.3.1 Uncoupled Heat Transfer Analysis

Uncoupled heat transfer analysis is generally employed to model heat conduction in a solid body with temperature-dependent conductivity, internal energy (including latent heat effects), or general convection and radiation boundary conditions, including cavity radiation. Since our model involves radiation and conduction modes of heat transfer, an uncoupled heat transfer analysis was employed. Non-linear heat transfer problems that arise due to temperature-dependent material properties, as in the present scenario, are solved iteratively in ABAQUS. A transient analysis was run on the model to

understand the behavior of thermal gradients in the assembly with respect to time. The result of the heat transfer analysis was stored in ABAQUS as a nodal temperature distribution with respect to time.

A solid model of the laminae stack was built in Solidworks and imported into ABAQUS for the analysis. A solid and homogenous section, which includes all temperature dependent material properties [1][8][22] (specific heat, density and conductivity), was created and each lamina in the stack was assigned with the section. An assembly of all the laminae was created. A hexagonal mesh was generated on all the laminae in the stack. Each stack had approximately 30,000 elements in it, with the size of each element being less than the smallest feature size in the stack. Figure 3-2 shows a representation of the test article with hexagonal mesh elements.

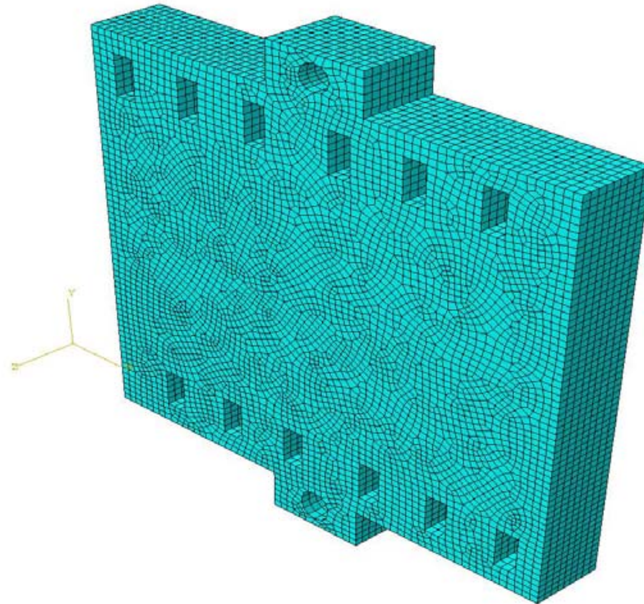

Figure 3-2. *Stack meshed with hexagonal mesh elements*

The transient heat transfer (HT) analysis was carried out in iterative loops for the initial 300 seconds of the ramp down thermal cycle to determine the time period and location of the maximum compressive thermal stresses during bonding. The transient analysis for the 300 seconds was conducted with a time increment of 0.01 seconds. For each increment, the temperature variation at each nodal point was recorded. The maximum variation of temperature for each increment was set at 50°C. The following assumptions were made for all analyses:

(i) The whole assembly is at bonding temperature (800°C) before the cooling cycle commences. This is because each of the diffusion bonding cycle has a dwell time of 60 minutes after ramp up, giving sufficient time for each assembly to stabilize at the bonding temperature.

(ii) All laminae are bonded perfectly since a uniform bonding pressure was applied to the assembly for 60 minutes at the bonding temperature to permit solid-state diffusion bonding [10].

(iii) The top and bottom surfaces of the stainless steel laminae stack are insulated since the stack is bounded by alumina platens.

(iv) All the laminae were perfectly flat.

The following boundary conditions were applied to the model:

(i) A pre-defined field of 800°C was enforced on the stack.

(ii) A tie constraint was applied to all laminae in the stack in order to impart bonded behavior within the assembly.

(iii) Heat transfer due to radiation would take place from the sides facing the heating elements.

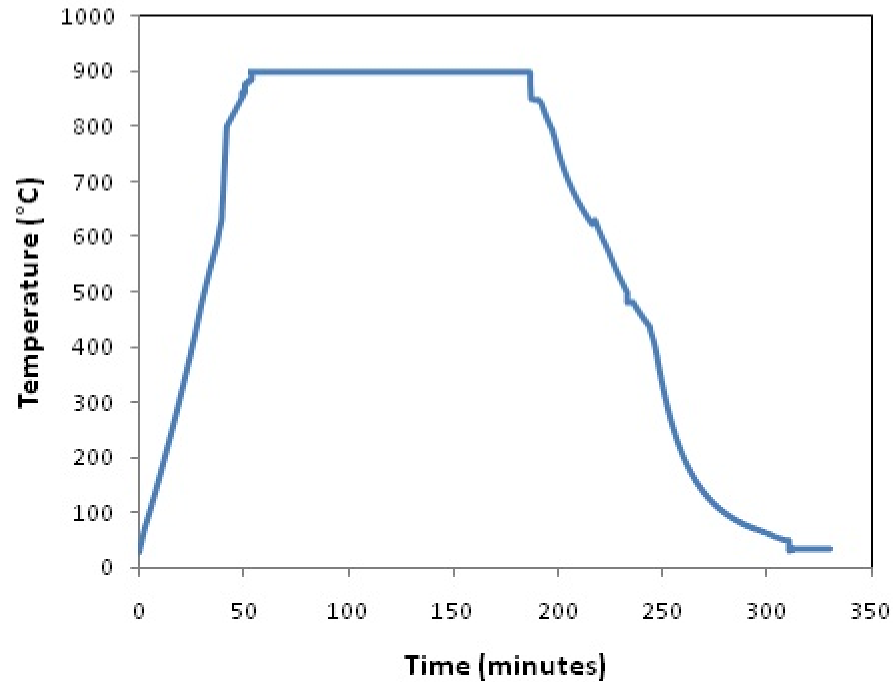

Figure 3-3. *Actual diffusion bonding cycle times of the sample [7]*

3.3.2 Transient Stress/Deformation Analysis

A mesh similar to the one used in the heat transfer analysis was produced in ABAQUS to conduct the sequentially-coupled transient stress analysis. This analysis was used to understand the thermal stresses developed in the laminae during the cooling cycle of the diffusion bonding process. A transient approach was chosen to understand the stress build-up in the assembly with respect to time.

The transient stress analysis was also performed in iterative loops for the first 300 seconds of the cooling cycle in conjunction with the heat transfer analysis to determine the maximum compressive stress that arises. The stress analysis was carried out by importing the nodal temperatures (output of HT analysis) as a predefined field. The nodal temperatures vary with position and time. The nodal temperature set was imported because it does not change by the stress analysis solution. The predefined fields are read into ABAQUS at the nodes and are then interpolated to the calculation points with the elements as needed. To define the temperature in the stress analysis with respect to position, the temperatures are stored at nodes. To define the temperature in the stress analysis at different times, the nodal temperatures are stored as a function of time in the heat transfer analysis results. It is necessary to maintain the same mesh type in both the heat transfer and stress analyses because ABAQUS assumes that the node numbers are the same for corresponding nodes in both the analyses. Temperature dependent material properties [1][8][22] (elasticity, plasticity, yield strength and co-efficient of thermal expansion) were fed into the model. The following assumptions were made for the stress analysis:

(i) The whole assembly is at bonding temperature before the cooling cycle commences.

(ii) All the laminae are perfectly bonded.

(iii) The top and bottom surfaces of the laminae stack are insulated.

(iv) Heat is lost from the stack only due to radiation.

(v) All the laminae are perfectly flat.

The following boundary conditions were applied to the stress analysis model:

(i) Nodal temperature set from heat transfer analysis was imported as a predefined field.

(ii) A pre-defined bonding temperature of 800°C was enforced on the stack.

(iii) A tie constraint was applied between all laminae to impart bonded behavior within the assembly.

(iv) No force was applied on the stack.

(v) A z-axis displacement constraint was enforced on the stack.

3.4. Preliminary Results

Preliminary heat transfer modeling results showed that the maximum thermal gradient was found to occur in the first few minutes into the cooling cycle. This corresponds to high rates of radiation taking place at higher temperatures of the test article according to:

$$P_{net} = A\sigma\epsilon(T^4 - T_c^4) \quad \text{(Equation – 5)}$$

where,

P_{net} = Power emitted by the body

A = surface area of the body (m^2)

σ = Stefan Boltzman's constant ($Wm^{-2}K^{-4}$)

ϵ = emissivity of the body

T = temperature of the body (K)

T_c = temperature of the surroundings (K)

Initial stress analysis results showed that the temperature gradients did not produce sufficient stresses required for thermal buckling of the fin. Upon closer examination, the thermocouple data revealed that the device underwent a much larger cooling rate than originally expected. Figure 3-4 shows a close-up of the thermocouple data for the first 60 seconds of the cooling cycle. A cooling rate of approximately 660°C/min can be seen at around 20 seconds. In order to match this high cooling rate, surface radiation to ambient boundary condition was substituted with surface heat flux to manipulate the cooling rate within the platen assembly. Since the exact location of the thermocouple was not reported in the study, a series of HT (and stress) analyses were conducted under various heat flux conditions that placed the desired cooling cycle at various places within the graphite platen. Assuming that the thermocouple was placed on the periphery of the graphite block, temperature profiles of the surface and the center of the fin are shown in Figure 3-5 for the heat flux boundary condition.

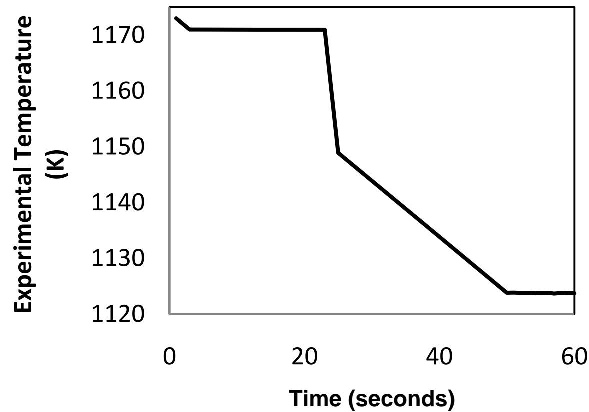

Figure 3-4. *Thermocouple data recorded for the first minute of cooling cycle [15]*

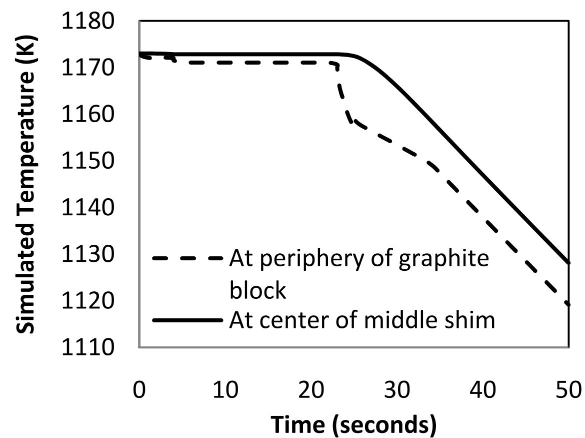

Figure 3-5. *Temperature profiles of the center and surface of the fin in the first minute of cooling cycle [15]*

Figure 3-6 shows the temperature distribution across the middle shim at the time of maximum thermal gradient (56°C/in.), which was found at approximately 24 seconds into the cooling cycle. The maximum temperature is at the center of the shim as expected because radiation heat transfer takes place on the periphery.

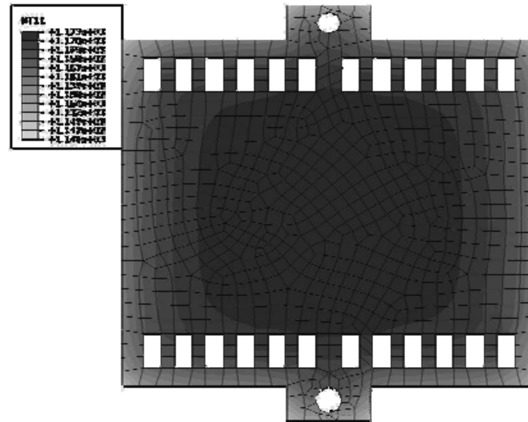

Figure 3-6. *Temperature distribution across the shim at an instant in the first minute of cooling cycle (thermocouple assumed to be on periphery of graphite block)[15]*

The transient stress analysis in ABAQUS showed that the highest compressive stress was also in the first minute of the cooling cycle. The maximum stress is in the middle shim towards the center (Figure 3-7). The maximum compressive stress achieved under these conditions (assuming thermocouple placement was on the graphite block periphery) was roughly 7 MPa. Figure 3-8 shows the stress profile of a node in the center of the middle shim with respect to time.

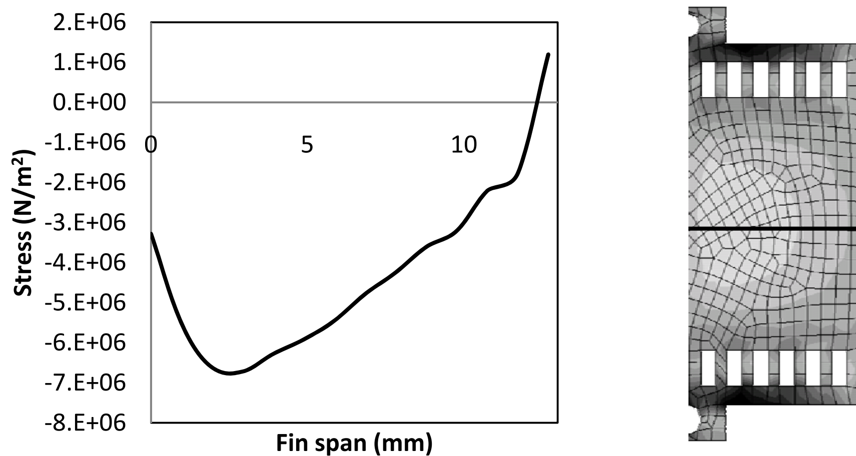

Figure 3-7. *Stress distribution across the fin at the instant of highest thermal gradient (thermocouple assumed to be on periphery of graphite platen)[15]*

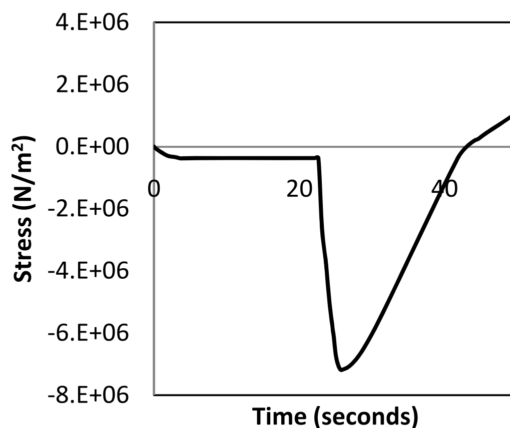

Figure 3-8. *Stress plot of a node at the point of maximum compressive stress in the middle shim (thermocouple assumed to be on periphery of the graphite block) [15]*

The analytically calculated value for the critical buckling stress of the fin was found to be 204 MPa which is significantly higher than those calculated in Figure 3-8. Since the exact location of the thermocouple was unknown, additional analyses were conducted with the same boundary conditions and assuming different locations of the thermocouple. To achieve the desired cooling rates within the microchannel structure, peripheral heat flux conditions were manipulated. Since the manipulation of surface heat flux boundary condition became difficult for thermocouple locations more than quarter inch from the periphery, stress values beyond that point were extrapolated. The extrapolated graph showed that stresses on the order of the critical buckling stress began appearing when the thermocouple location was assumed to be one half inch from the periphery of the graphite platen. Figure 3-9 & Figure 3-10 represent the temperature and stress distributions respectively across the fin for the thermocouple position assumed to be quarter inch from the periphery.

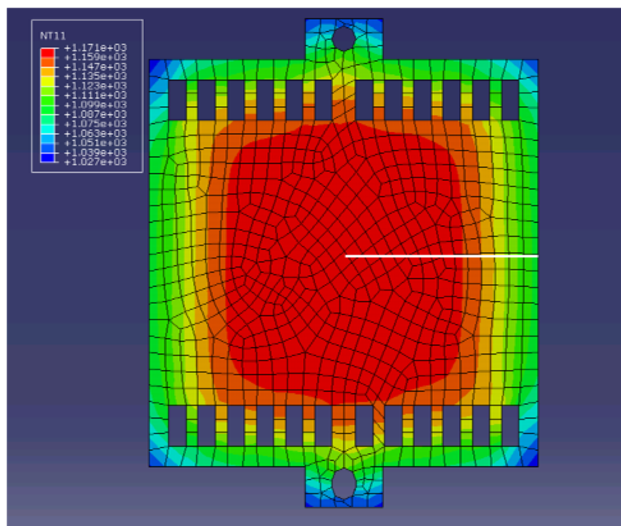

Figure 3-9. *Temperature distribution across the middle shim at an instant in the cooling cycle (thermocouple assumed to be half inch from edge of graphite platen)*

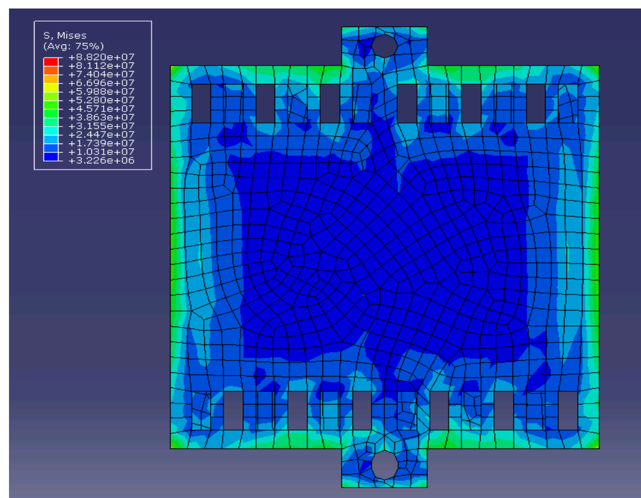

Figure 3-10. *Stress distribution across the middle shim at an instant in the cooling cycle (thermocouple assumed to be half inch from edge of graphite platen)*

CHAPTER 4

4. EXPERIMENTAL APPROACH

4.1. Overview

FEA was employed in this study to predict the conditions leading to thermal buckling of microchannel fins in test articles. An earlier study [33] demonstrated an approach to finite element modeling for investigating the cause of warpage within microchannel structures produced under different heating and cooling conditions. However, results were inconclusive since the precise thermocouple location for those experiments was unknown. Consequently, in this thesis additional experiments were conducted to validate finite element models and provide insight into the limits of cooling rates in the diffusion bonding of metal microchannel structures.

All equipment used in experiments was calibrated using standard procedures before conducting experiments. A load cell of 0-5000 pounds range capability was used to calibrate the applied pressure in vacuum hot press. Fuji pressure sensitive film was used to validate the pressure uniformity and parallelism of the ceramic platens. Profiler and optical microscope were calibrated using dimensional standards and used to measure the warpages of diffusion-bonded test articles.

4.2. Test Article Design and Material Selection

The goal of the experiment was to establish a relationship between the critical

buckling stress, lamina thickness and cooling rates for fabrication of microchannel devices. A test article concept was developed which could be used to rapidly assess the warpage of a microchannel fin due to transient thermal gradients that arise during diffusion bonding. The test article consisted of 3 layers made from copper alloy 110. Copper was selected as the material for study, since it has a low modulus of elasticity and yield strength at higher temperatures which are necessary for producing thermal buckling behavior with small test articles. The mechanical properties of copper reduce drastically near the bonding temperatures [21][29]. In addition, copper is readily machinable using laser patterning techniques which were readily accessible. Finally, copper has been diffusion bonded across a wide range of bonding parameters [10].

The test article consisted of a fin layer sandwiched between two channel layers (Figure 4-1). The top and bottom copper channel laminae were 25.4 x 25.4 x 0.2 mm. The middle copper fin lamina also had a length and width of 25.4 x 25.4 mm. The thickness of the middle lamina was varied from 0.05 to 0.2 mm. Alumina platens with dimensions of 50.8 x 50.8 x 12.7 mm were used to apply pressure to the test article. The fin and channel layers were designed in such a manner so that fin warpage could be rapidly assessed with the use of a profiler.

FEA was used to determine the length, width and thickness of the channel and fin layers to cause the expected warpage behavior. To reduce the number of experimental runs, multiple test articles were run for each bonding cycle. Different dimensions of the test articles used in this study are presented in Appendix A. Bonding platens made of alumina were used on the top and bottom sides of the test article for transmitting bonding

pressures uniformly in the vacuum hot press. These alumina platens (manufactured by Coorstek) have a very low thermal conductivity value and work as insulators impeding heat flow through the top and bottom of the laminae stack. The platens were designed to be 50.8 X 50.8 x 12.7 mm and were double side grounded to have good flatness and parallelism. The parallelism of the blocks is less than 10 μm over the whole surface and surface roughness was observed to be less than 0.5 μm.

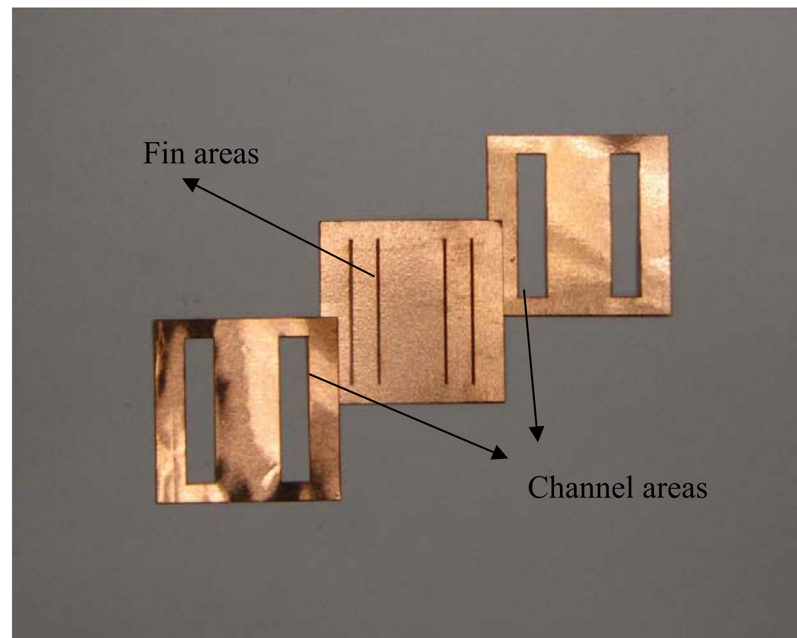

Figure 4-1. *Test article used in this study with channel and fin areas*

Mechanical and structural properties of copper alloy 110 shimstock, used in experiments, at room and bonding temperatures are presented in Table 4-1.

Table 4-1. Mechanical properties of copper alloy 110 at room and bonding temperatures

Properties	Room temperature (25°C)	Bonding temperature (800°C)
Young's modulus (E)	1.15×10^{11} [N/m^2]	25×10^{11} [N/m^2]
Poisson's ratio (ν)	0.343	0.3

4.3. Test Article Fabrication

4.3.1 Laser Machining

Each test article used for the study consisted of three layers: one fin layer and two-channel layers. The fin layer was sandwiched between the two channel layers. All the layers of the test article were made of copper shim stock alloy 110 (annealed temper, 99.9% copper). For all the experiments conducted, the channel layers were 200 µm thick whereas fin layers are made of four thicknesses (50, 75, 100 and 200 µm). An ESI 5530 Nd: YAG laser machine manufactured by Electro Scientific Industries (ESI) was used to cut the shim stock with the desired features. The laser machine operates at the second harmonic (532nm) with a maximum power output of 5.8W. Cutting speed, pulse frequency, z-offset and the number of repetitions were modified and adjusted as needed for different thicknesses shim stock. High cutting speed and low number of repetitions were used to reduce the thermal stress during the pattering operation. Figure 4-2 shows a comparison of features cut with non-optimized and optimized laser parameters.

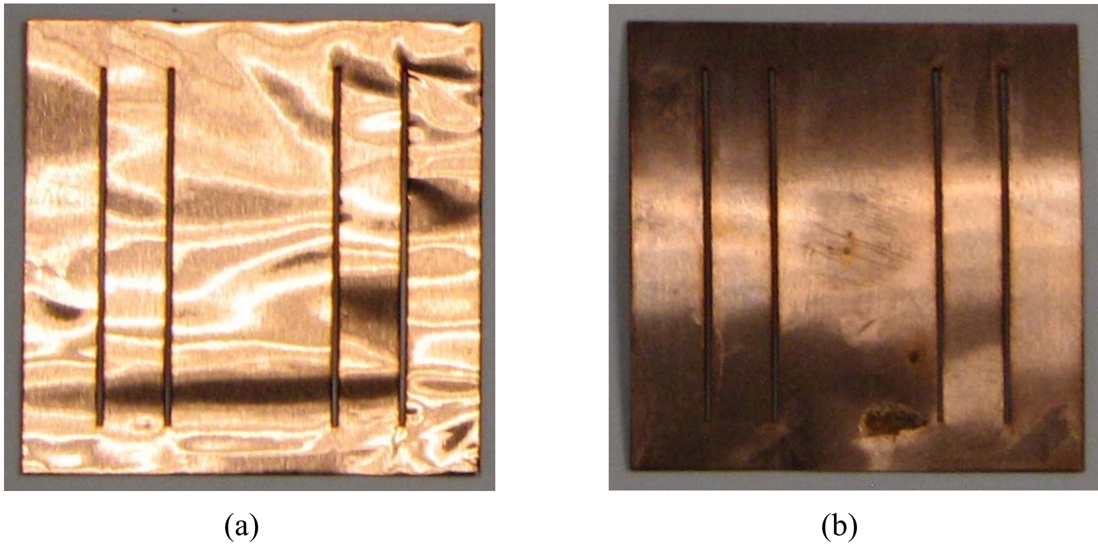

(a) (b)

Figure 4-2. *Warpage in lamina after patterning features on the laser using (a) non-optimized parameters, (b) optimized parameters*

G-code needed for the laser machine was developed using SmartCAM (Advanced Fabrication v.15) software. Listed below in the Table 4-2 are the parameters used for patterning the copper laminae on the laser.

Table 4-2. *Laser parameters used to pattern features on the copper laminae*

	50 µm				**75 µm**				**100 µm**				**200 µm**			
Z-offset (mm x 10^{-2})	0	15	30	40	0	20	40	55	0	25	50	75	0	50	100	150
Speed (mm/s)	100				100				100				100			
Repetition rate (KHz)	30				30				30				30			
Power (W)	5.8				5.8				5.8				5.8			
Repetitions	2	2	1	1	2	2	2	2	3	3	3	3	10	10	10	10

4.3.2 Deburring

A contact profiler (Veeco Dektak 3) was used to evaluate the flatness and burr height of the patterned laminae after laser machining. The profiler was equipped with a 12.5 µm diamond tipped stylus with a capability of measuring a minimum z-dimension of 50 nm. Laser burrs, caused by deposition of laser ablation ejecta, were found and measured at three different locations on each of the lamina and the average value was found to be 5.9 µm with a standard deviation of 1.1 µm. Figure 4-3 shows the locations of scans, where the measurement of laser burrs on the laminae were taken.

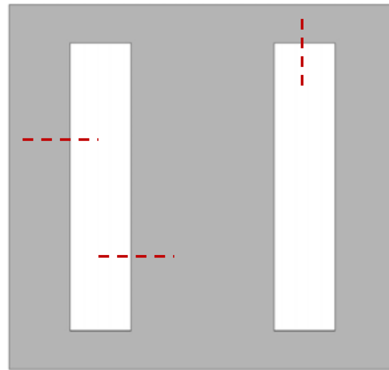

Figure 4-3. *Scan locations on the test articles for laser burr*

Burrs were removed in a systematic process so as to create intimate contact between the fin and channel laminae during diffusion bonding process. The deburring process involved polishing laminae with 3M Scotch-Brite^{TM} followed by cleaning in an ultrasonic bath of citronox and de-ionized water for 20 minutes. Figure 4-4 shows representative profiler scans of the laser burrs before and after deburring and flattening.

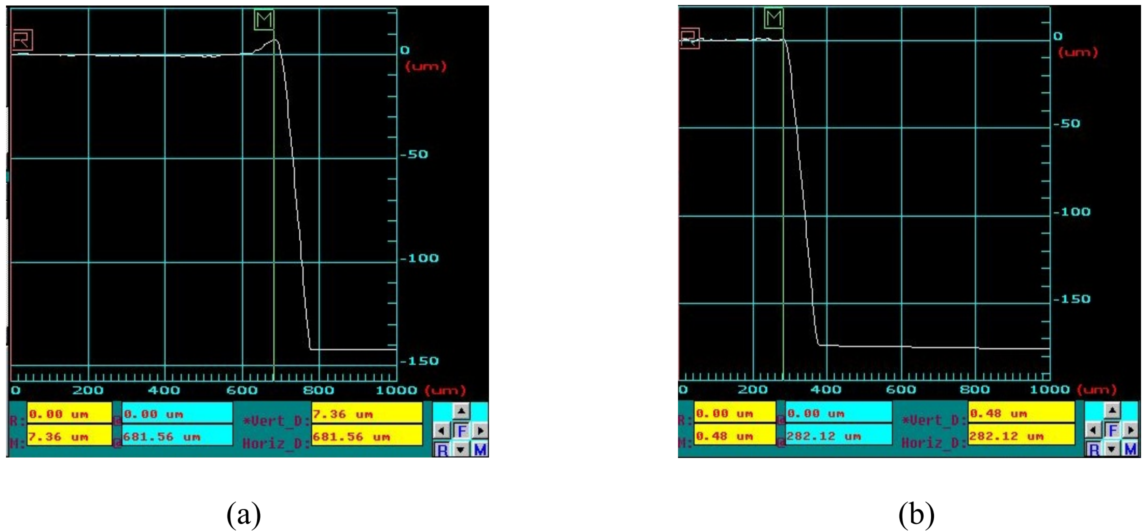

(a) (b)

Figure 4-4. *Profiler images of laser burrs (a) before and (b) after flattening cycle*

4.3.3 Flatness

The Dektak profiler was used to run two scans perpendicular to each other, each for a length of 10mm on all the samples to measure the flatness and surface roughness. The measurements showed an average surface roughness of 0.22 µm with a standard deviation of 0.09 µm, which is well within the limit of 0.4 µm desired for diffusion bonding of laminae.

4.3.4 Buckling Criteria

Buckling models are usually categorized based on the initial state of the column (or plate) as being linear (small initial deformation relative to thickness of the material) or

non-linear. Based on the lamina flatness achieved, the model problem developed in this study is considered to be linear i.e. the plate is considered to be without imperfections. In this straight forward case, the compressive stress, P_c, for a column under compression from an initial length L1 to a final length L2, is given by:

$$P_c = \frac{4\pi^2 EI}{L_c}$$

In linear theory, buckling does not happen until P_c is greater than or equal to the critical buckling stress (σ_c). The deflection function of the fundamental mode when σ_c [39] is achieved is given by

$$w = \frac{1}{2} w_{max}(1 - \cos\frac{2\pi x}{L})$$

where,

w_{max} = maximum amplitude

L = length of the beam

x = distance from fixed end

While we are not considering the magnitude of deflection in our study, the question arises, at what point is the plate considered buckled? From the literature, it is recognized that flow maldistribution effects in microchannel arrays becomes pronounced at channel deviations of 10% [4]. In this study, the thickness of test article coupons was between 50

and 200 µm. Therefore, deflections beyond 10% of the lamina thickness were considered as buckling.

4.3.5 Flattening

In order to establish initial flatness of the laminae, the patterned and deburred laminae were placed in-between graphite platens and run through a flattening cycle. This cycle along with flattening the samples, also serves in relieving any residual stresses from the cold rolling process. During the flattening cycle the laminae were raised to a temperature of 500°C and a pressure of 2.5 MPa (350 psi) was applied for 30 minutes. The cycle was run in a vacuum hot press under 10^{-4} torr vacuum to prevent any oxidation of the copper laminae. The flatness of the laminae was then measured by scanning the laminae over a length of 20mm using Dektak profiler. The flatness across the laminae was found to be approximately 3 µm with a standard deviation of 0.2 µm after flattening. Note that this flatness is below the buckling threshold outlined above.

4.3.6 Bonding

Before bonding, all the laminae were stacked in a wafer holder and cleaned in the ultrasonic cleaner with acetone, methanol and de-ionized water (AMD rinse) to remove any grease and residues on the faying surfaces to have good bonding. After ultrasonic

cleaning, the laminae are dried in a vacuum oven for 20 minutes to remove any moisture on the surfaces. The laminae are then aligned between the alumina platens using alignment pins and then diffusion bonded.

4.4. Load Cell Validation

One of the important settings needed for this study was the magnitude of bonding pressure applied on the stack during the diffusion bonding process. Diffusion bonding of the laminae is usually performed in a vacuum hot press and the bonding force is applied using the hydraulic rams present inside. Since a high pressure induces lateral stresses in the stack due to Poisson's effect [9], which may affect the understanding of warpages, the hydraulic rams were calibrated using a load cell before the experiments were conducted. A load cell with a calibration range of 0 – 5000 pounds manufactured by Omega was used to calibrate the force applied by the hydraulic rams. The excitation of the load cell is rated as 10V maximum, i.e., a force of 5000 pounds represent a voltage read out of 10V and 0 pounds represent voltage readout of 0V. A linear relation has been established between the GUI read out of the vacuum hot press and the actual applied load. Figure 4-5 shows the relation between the GUI reading on the vacuum hot press and the actual load applied.

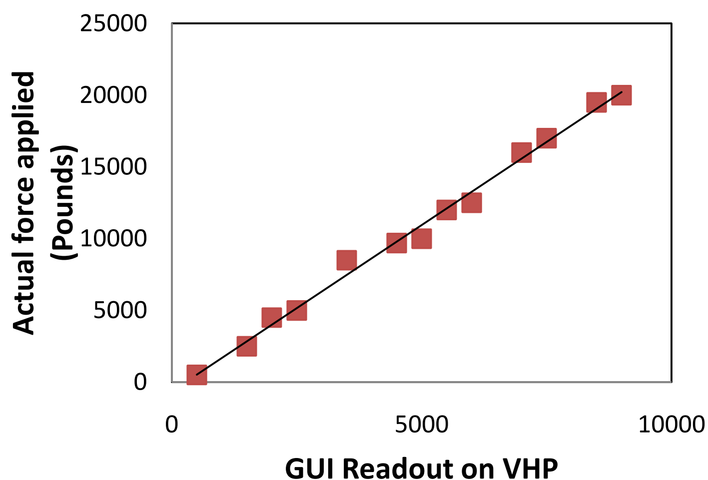

Figure 4-5. *Relation between hot press GUI readout and load cell reading*

4.5. Experimental Design

Cooling rates and laminae thicknesses used in the analyses are shown in 0. Cooling rates of less than 2°C/min were not considered because it could not be replicated experimentally, since the minimum cooling rate that could be achieved in the vacuum hot press was 2°C/min.

Table 4-3. *Cooling rates at which the experiments were conducted*

<table>
<tr><th>Fin thickness (μm)</th><th>Cooling rate (°C/min)</th></tr>
<tr><td rowspan="3">50</td><td>2</td></tr>
<tr><td>3.5</td></tr>
<tr><td>14</td></tr>
<tr><td rowspan="2">75</td><td>2</td></tr>
<tr><td>11</td></tr>
</table>

	14
100	3.5
	5
	10
200	8
	12
	14

4.6. Thermocouple Set-up

Efforts were made to validate the temperature in the cylinder of the vacuum hot press. For validating the temperature readout of the thermocouples, temperature of a location in the vacuum chamber was verified with different thermocouples. The maximum difference in the readout was 2ºC. As other data point sets, temperature of ice and boiling water were measured using all the thermocouples. All the thermocouples measured accurately and the maximum difference in the readings of the thermocouples was 1.5ºC.

A total of four thermocouples were installed to monitor the temperature of interest inside the hot zone. Flexible K-type thermocouple wires were inserted through the vacuum manifold up into the hot zone as shown in Figure 4-6. The thermocouples have a high temperature insulation coating to protect the inside from high temperatures of the

vacuum hot press. The ends of the thermocouples are connected to thermocouple elements that are in-turn connected to a thermal data logger. A 4-inlet temperature data logger manufactured by Sper Scientific Ltd. (type 800024) was used to record the thermocouple readings. The instrument has a working range of -200°C to 1370°C with a resolution of 1°C or 1 second and an accuracy of ± 0.2% based on the reading. The temperature conversion of the instrument follows National Bureau of Standards and IEC584 temperature/voltage table for type K thermocouples. The data logger has an internal storage capacity to store 16000 readings per inlet and can be connected to PC over a RS232 interface and TestLink SE-309 software.

One of the thermocouples, placed on the surface of the stack, was used to send feedback of the temperature to the eurotherm of the heating element circuit. Another thermocouple was placed on the opposite surface of the stack to ensure uniform heating of the stack on all sides. Figure 4-7 shows the Solidworks model of a ceramic platen representing the locations of the thermocouples. Figure 4-8 shows actual thermal data logger readings for various cooling rates used during experimentation.

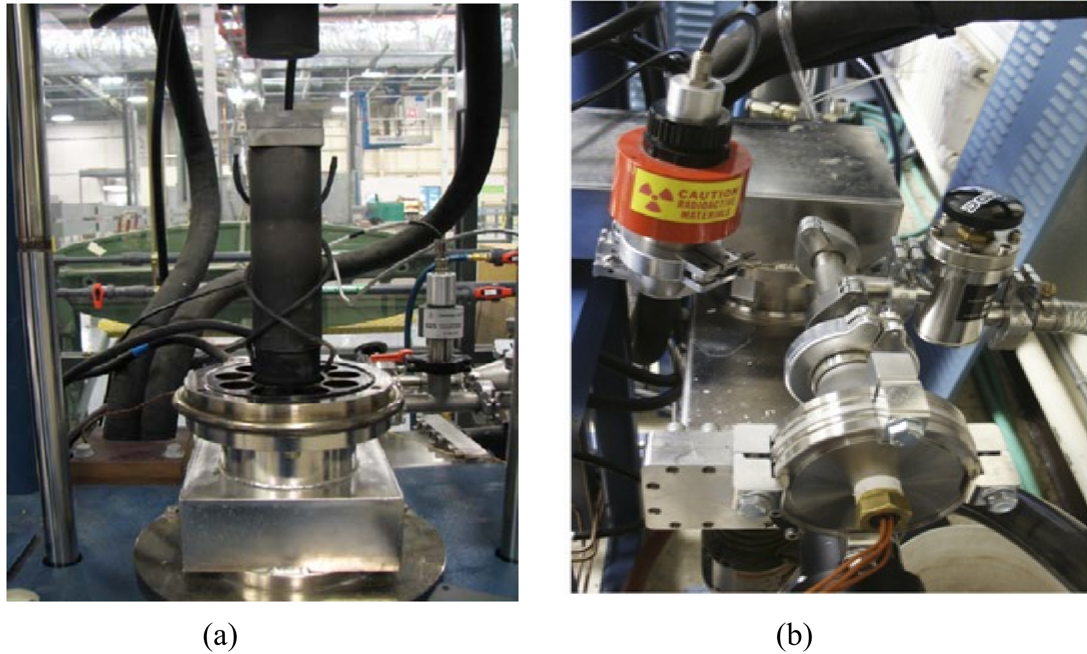

(a) (b)

Figure 4-6. *(a)Location of thermocouples in the vacuum chamber (b) Vacuum port in which thermocouples are connected to thermocouple elements*

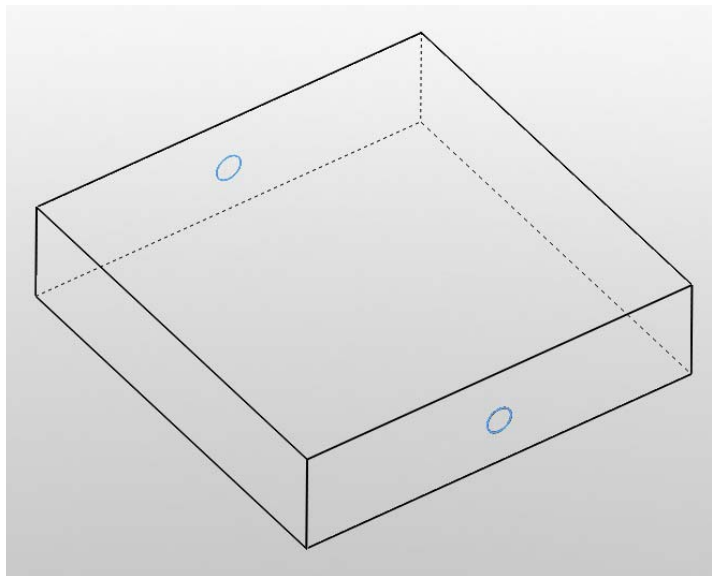

Figure 4-7. *Locations of thermocouples in the ceramic block*

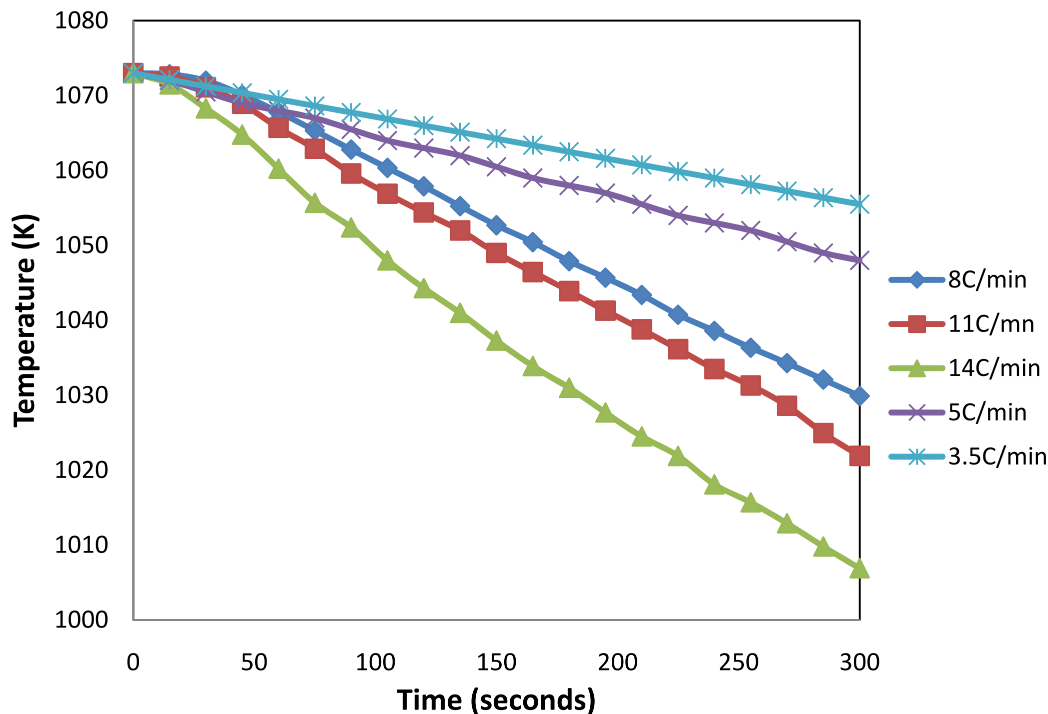

Figure 4-8. *Thermal data logger graphs showing the actual cooling rates of the stack during diffusion bonding cycles*

4.7. Pressure Uniformity with Fuji Pre-scale Film

Uniformity of the applied pressure is strongly dependent on the machining quality of the bonding platens and the hydraulic rams; especially their parallelism. Therefore, the alumina bonding platens used in this study were tested on their ability to distribute the pressure uniformly. Pressure sensitive film (Fuji Prescale type LW) was used to test the pressure distribution of the top and bottom bonding platens. Initial results showed that there was a variation of pressure in the platens. Figure 4-9 shows the non-uniform pressure distribution of the platens on the pressure sensitive films. Parallelism was measured using a surface profiler and a noticeable variation was seen. The peak to valley

measurement was measured to be roughly 8µm. The platens were ground using 1µm sand paper to remove the variation of thickness.

Figure 4-9. *Pressure distribution of the platens measured using sensitive films before machining*

Re-machining of the parts significantly reduced the peak to valley surface waviness to about 2µm. Pressure distribution experiment with the pressure sensitive film was repeated to see the effects. It can be seen from the pressure film readings that the pressure is distributed uniformly across the platens. Readings were taken for different pressure ranges. Figure 4-10 shows the pressure distributions of the films the various pressures applied.

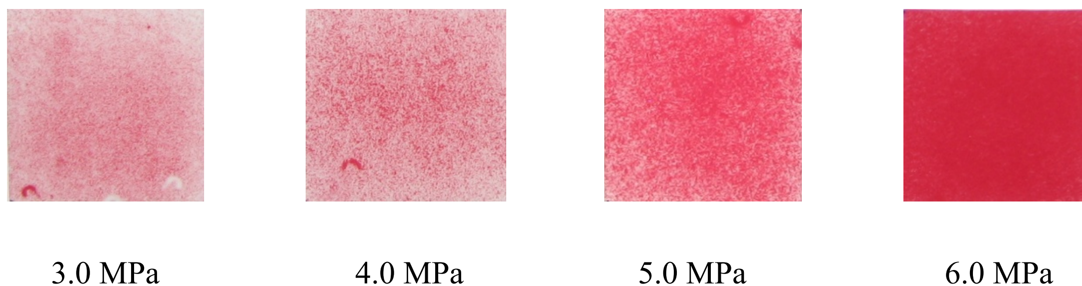

Figure 4-10. *Pressure distribution of the platens measured using sensitive films*

The ceramic platens were coated with a thin layer (~1 µm) boron nitride (ZYP) to avoid any frictional adherence of the stack to the platens. Since the coating was laid

manually, pressure distribution test with pressure sensitive films was repeated for bonding pressure. Figure 4-11 shows the representation of pressure distribution with ZYP coating on the platens.

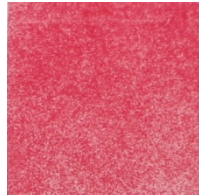

5.0 MPa

Figure 4-11. *Pressure distribution of the platens with ZYP coating*

4.8. Diffusion Bonding Cycle

Diffusion bonding of laminae is a solid state joining process, in which two cleaned and smooth surfaces are pressed at elevated temperatures to form a monolithic device. Bonding is usually done in a controlled atmosphere or in high vacuum to prevent oxidation of laminae which acts as a barrier for bonding. No matter what process is employed to machine the parts, it presents a microscopically rough surface. So, for diffusion bonding of materials, the laminae are to be heated to bonding temperatures, typically 0.5 – 0.7 Tm (melting temperature). Elevated temperatures reduce the yield stress of materials and activate diffusion and mobility of atoms. The inter-atomic forces of attraction begin to be felt at distances between 10^{-4} and 5.10^{-4} µm.

Experiments were conducted to understand the warpage mechanism in microchannels during heating to and cooling down from bonding temperature. Higher

rates of heating / cooling induce thermal gradients in the body which induce thermal strains which raise thermal stresses in the body. At elevated temperatures, since the yield stress of the material is low, the laminae tend to deform at lower thermal stresses. Experimental runs were designed by selecting different cooling rates and laminae thicknesses. Four different thicknesses (50, 75, 100 and 200 µm) of copper shims were chosen to conduct the experiments and to relate the thickness of lamina to cooling rate. Cooling rates were decided for each thickness based on finite element analyses data.

After flattening and cleaning cycles, the patterned shims were stacked and aligned using alignment pins. Each stack consisted of a fin layer bounded by two channel layers. The assembled shim stack was placed in between two alumina platens of sizes 50.8 X 50.8 X 12.7 mm. These platens acted as insulators on the top and bottom of the shim stack leaving only the sides as path for heat (input / output) due to radiation. The platens were coated with a thin layer (~ 1 µm) of boron nitride (ZYP coating) to avoid any adherence of shims to the alumina platens. Four thermocouples were placed: two at the surfaces of alumina platen, one at a depth of quarter inch from the side of alumina platen and one at a depth of half inch from the side of alumina for understanding the temperature distribution across the chamber. Temperature data was logged for all the thermocouples using a Sper temperature data logger with a time interval of 1 second during the cooling cycles.

Bonding parameters for diffusion bonding the laminae were temperature = 800°C; heating rate = 20°C /min; dwell time at bonding temperature = 90 minutes; bonding pressure during dwell time = 7MPa. A high vacuum of 10^{-5} torr was maintained in the hot

press throughout the bonding cycle to avoid any oxidation of materials.

Each thickness of the fin layer was run at three different cooling rates to estimate the cooling rate at which warpage appears. For each thickness of the lamina, one cooling rate is chosen which does not warp the material, one which warps the material and one that would raise just enough thermal stresses in the body to cause warpage. Estimation of these cooling rates for the runs was based on the finite element analyses data. Cooling rates with respect to thicknesses are mentioned in the Appendix.

CHAPTER 5

5. RESULTS AND DISCUSSION

5.1. Critical Buckling Stresses

As a baseline for the FE analyses, analytical values for critical buckling stresses needed for fin warpage were calculated using the formula described in section 2.4.2. The table below shows the critical stress values needed for different thicknesses of fins to cause buckling. (Calculations were made using material properties at bonding temperature.) To validate thermal buckling conditions, thermal compressive stresses developed during the bonding process must exceed the critical buckling stresses shown in Table 5-1 leading to warpage in the test article that could be measured using the contact profiler.

Table 5-1. *Critical buckling stresses for fin buckling with respect to thickness*

Thickness of the fin (μm)	Critical buckling stress (MPa)
25	0.1410
50	0.5819
75	1.3094
100	2.3279
125	3.6374
175	6.9127
200	9.3118

5.2. Finite Element Analysis Results

FEA analysis was conducted for each lamina thickness with different cooling rates to determine the minimum cooling rate that would induce thermal buckling in the fin. It can be observed from the Figure 5-1that compressive stresses are generated during the cooling cycle.

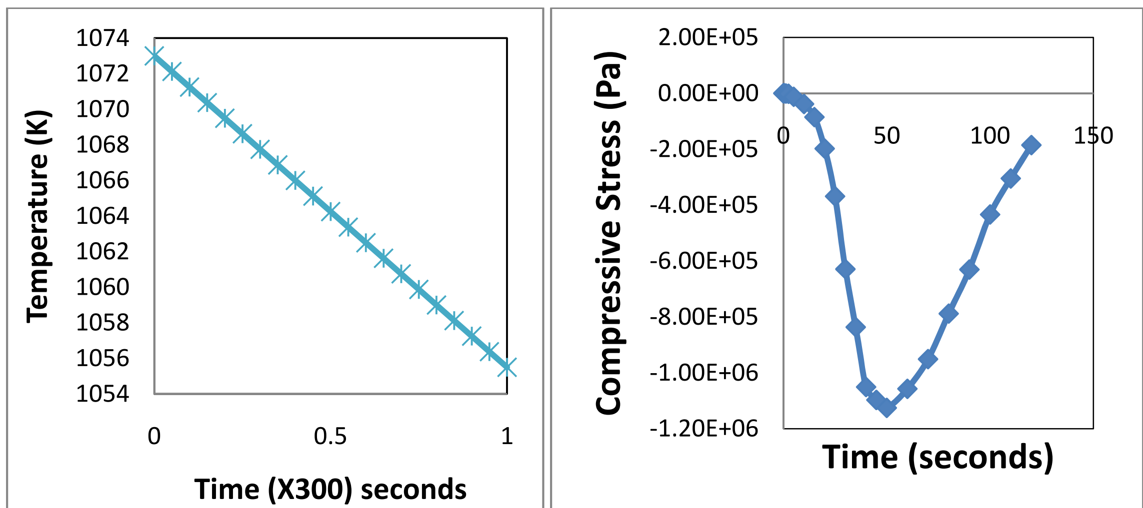

Figure 5-1. *Temperature and stress profiles for a lamina thickness of 100 µm cooled at a rate of 3.5 ℃/min*

FEA results showed that for laminae thicknesses of 50 and 75 µm, cooling rates less than that achievable in the vacuum hot press (2°C/min) were found to produce stresses greater than the analytical values needed for fin buckling. At a 2°C/min cooling rate, the maximum compressive stresses generated within the fin area under consideration for 50 and 75 µm thicknesses were ~1.2 and ~1.7 MPa, respectively. These are greater than the analytically calculated values of 0.58 and 1.31 MPa, respectively.

FE analysis conducted with a cooling rate of 3.5°C/min on a 100 μm thick lamina generated compressive stresses of approximately 1.93 MPa in the fin region. This value is less than the analytically computed value of critical buckling stress (2.33 MPa) needed for fin buckling. In contrast, analyses at 5 and 14°C/min suggest fin buckling. Figure 5-2 (a) and (b) show temperature and stress distributions in the fin a few seconds into the 5°C/min analysis. Stresses above 2.33 MPa (analytical value of buckling stress) can be observed.

FE analyses were conducted for a lamina thickness of 200 μm at cooling rates of 8, 11 and 14°C/min. Results showed that the stresses developed at 8 and 11°C/min are only 60% and 85-90% of the critical buckling stress value computed analytically. At a cooling rate of 14°C/min, the maximum compressive stress generated in the fin area exceeded the analytical value of the critical buckling stress.

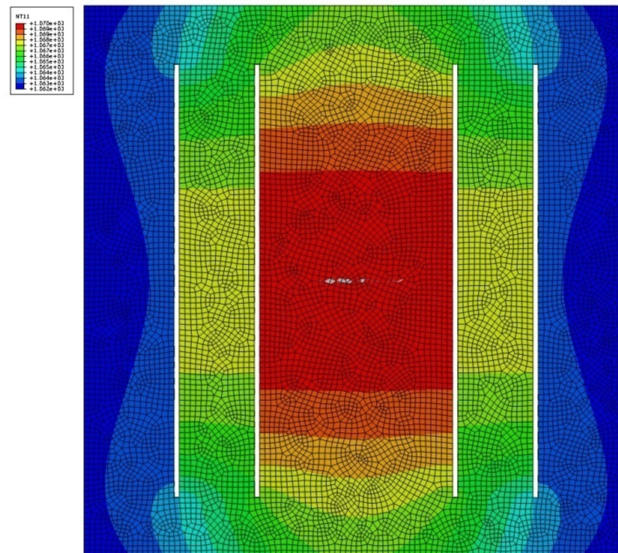

(a)

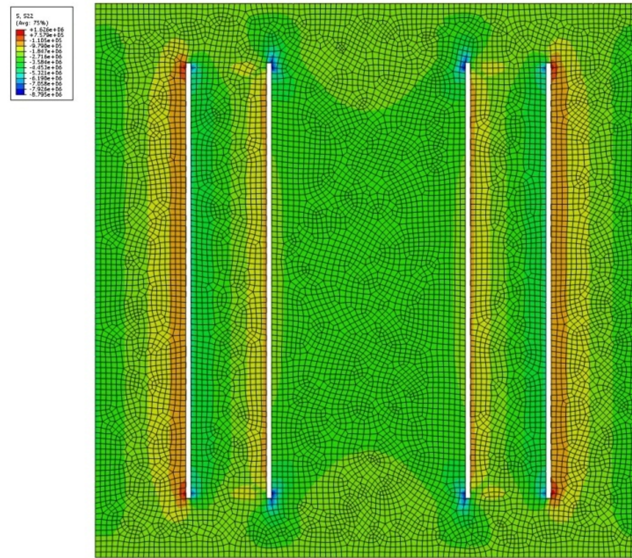

(b)

Figure 5-2. *(a) Temperature distribution and (b) stress distribution in 100µm shim, run at a cooling rate of 5°C/min*

5.3. Experimental Results

Based on the FEA results, experiments were conducted for all the laminae thicknesses and cooling rates mentioned in Table 4-3. Figure 5-3 represents the experimental data (cooling rate vs. lamina thickness) collected in this study. Each fin thickness was diffusion bonded at three different cooling rates. Cooling rates were chosen based on finite element results suggesting where thermal buckling should happen for a particular lamina thickness. In order to measure the fin buckling, profiler scans were made across the fin length at three different locations on each fin. The solid dots represent experimental runs in which the fins were found to be buckled using the

established buckling criteria and hollow dots represent the runs in which the fins were not buckled.

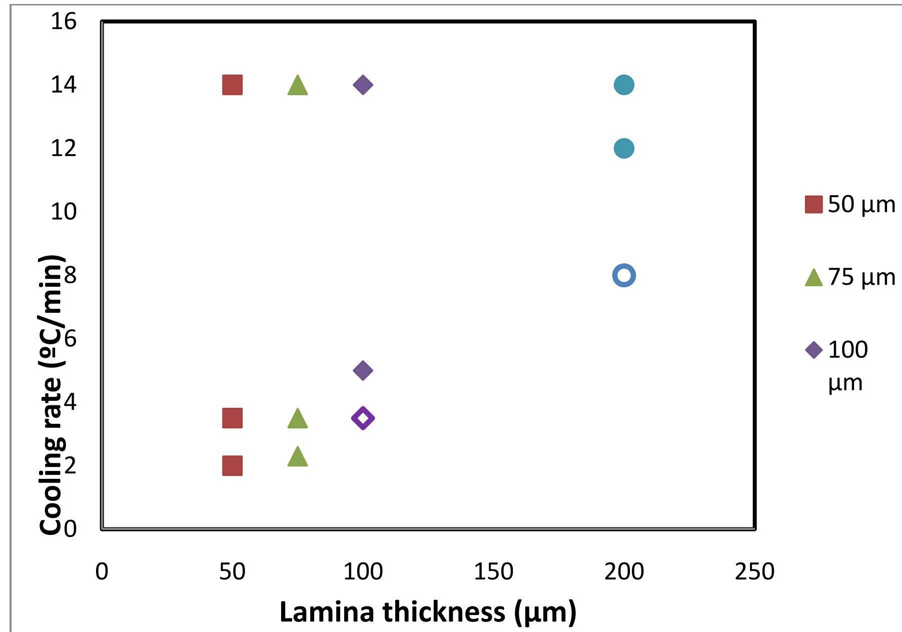

Figure 5-3. *Experimental runs showing buckled and non-buckled lamina thickness with respect to cooling rate*

Figure 5-4 represents a comparison of the FEA predicted stress values for fin buckling and the experimental results. FEA results are plotted in blue and overlaid on the previous experimental results. FEA results were established by running simulations with different cooling rates. For a given lamina thickness, a point was plotted when the maximum thermal stress at a particular cooling rate was found to be within ±10% of the critical buckling stress for that lamina thickness. Therefore, the curve in the figure is the approximate loci of FEA predicted cooling rates with respect to lamina thickness for the onset of buckling. The form of this equation is consistent with the fact that the critical buckling stress varies with the square of the lamina thickness

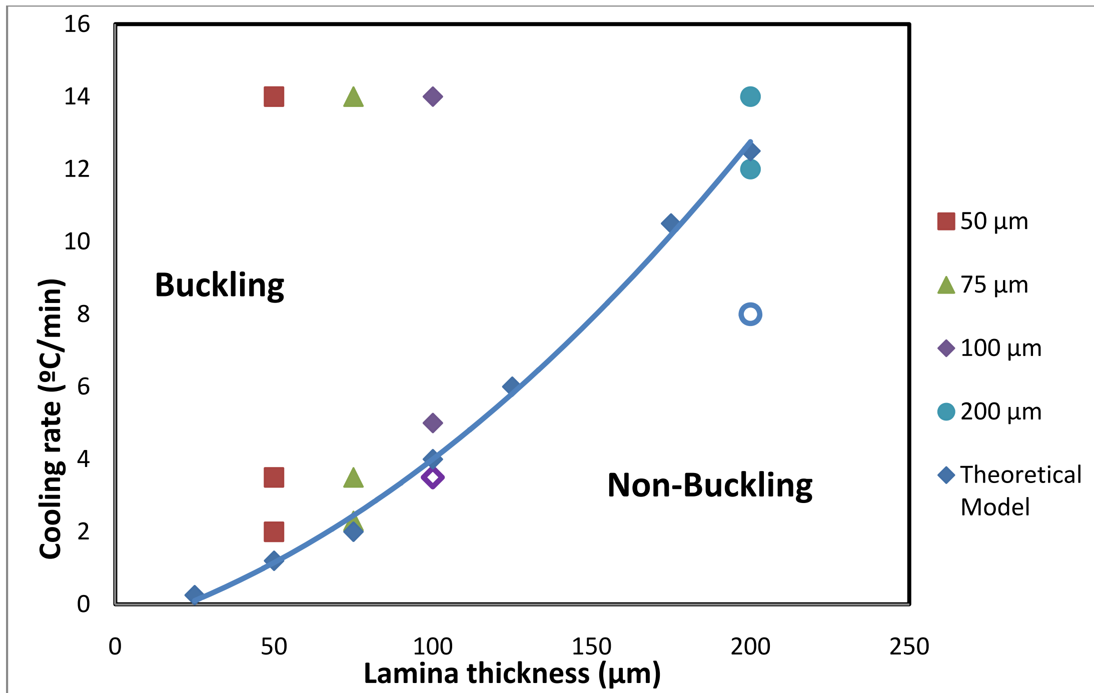

Figure 5-4. *Comparison of FEA predicted cooling rates where thermal stresses equal to critical buckling stress*

5.4. Discussion

The area above the curve (labeled as "Buckling") in Figure 5-4 represents the cooling rates with respect to lamina thicknesses where buckling of fin occur during diffusion bonding. It can be seen from the figure that the experimental results are in general agreement with the FEA analyses. This can be observed in particular for laminae of 100 and 200 µm thicknesses cooled at 3.5 and 8ºC/min, respectively, where no buckling was predicted or found.

For a lamina thickness of 50 µm, an average z-deflection of approximately 100 µm was observed which is well beyond the buckling criteria. For a lamina thickness of 75 µm, the z-deflection was observed to be approximately 100 µm when the stack was cooled at the rate of 2°C/min and 125µm when cooled at the rate of 3.5°C/min. It can thus be concluded that for cooling rates of 2ºC/min and above, buckling occurs in 50 and 75 µm thick microchannel laminae due to compressive thermal stresses.

In the case of 100 µm lamina thickness, the stack diffusion bonded at the cooling rate of 3.5°C/min, the fin area under consideration had minimal or no deflection. Profiler scans across the fin length showed a maximum z-deflection of approximately 5 µm which is below the buckling threshold of 10%. These results agree with the FEA results above, suggesting that the thermal stresses at this cooling rate did not exceed the analytically computed critical stress value. Figure 5-5 shows the profiler scan for 15mm of the fin length.

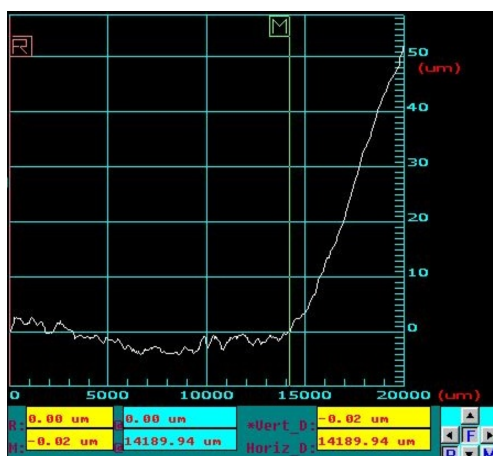

Figure 5-5. *Profiler scan over a length of 15mm on the fin of thickness 100µm cooled at a rate of 3.5°C/min*

For the 100 µm thick laminae stack diffusion bonded at the cooling rate of 5°C/min, the maximum z-deflection in the fin region was observed to be approximately 100 µm, qualifying it as fin buckling. This is in agreement with FEA results above. Figure 5-6 shows the profiler scan across the fin length. It is interesting to note that the deflection was a sinusoidal wave-like curve suggesting multi-mode deflection. This could mean that the amount of deflection was so great that it interfered with the bonding platens leading to the multi-mode deflection pattern.

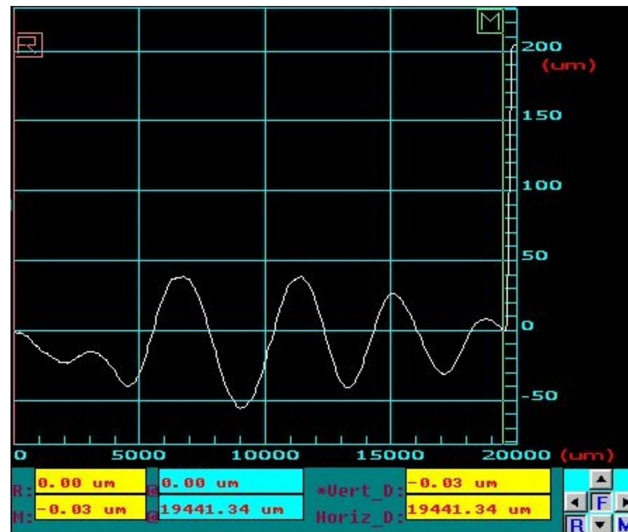

Figure 5-6. *Profiler scan over a length of 15mm on the fin of thickness 100µm cooled at a rate of 5 °C/min*

For a fin thickness of 200 µm, diffusion bonding cycles were run at cooling rates of 8, 12 and 14°C/min. The maximum z-deflection in the fin region for the stack run at

8°C/min was less than 6 µm. This is less than 10% of the fin thickness suggesting that no buckling had occurred.

For cooling rate of 12°C/min, the profiler scan showed a z-deflection of 100 µm, which is of the order of shim thickness. FE results for this cooling rate generated approximately 85-90% of the critical buckling stress needed for fin buckling. The deflection at a little lower cooling rate can be attributed to deviation in flatness of the fin before diffusion bonding cycle. It has been reported that approximately only 80% of yield stress is necessary for warping a fin with initial deviation in flatness [2].

5.5. Sensitivity Analysis

To better understand the buckling behavior of microchannels during diffusion bonding, finite element analysis was extended for a different fin span. A fin span of 10 mm was chosen keeping the other independent variables (width, thicknesses and cooling rates) constant. Figure 5-7 shows a graph representing the sensitivity analysis data for different lamina thicknesses with respect to cooling rates. From the figure it can be observed that the cooling rates needed for fin buckling of 10 µm laminae were exponentially higher than the cooling rates needed for buckling 20 µm fins. This can be attributed to higher critical buckling stress needed to buckle the lamina. It can be seen from Equation – 4 that critical buckling stress increases in second order with respect to lamina span.

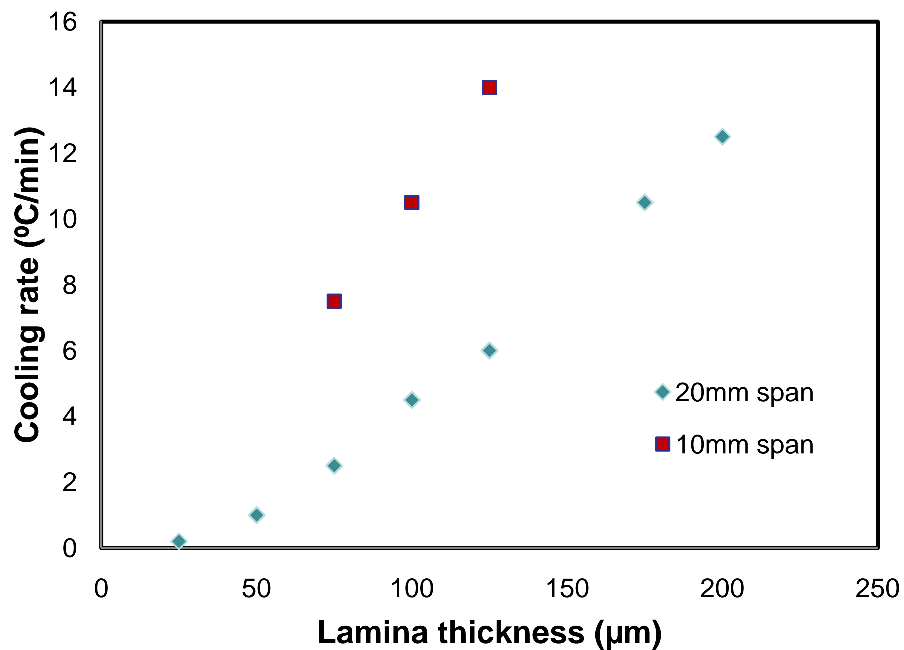

Figure 5-7. Cooling rates comparison for different fin spans

CHAPTER 6

6. CONCLUSIONS

A finite element model was developed to predict thermal stresses within microchannel fins as a function of the cooling cycle in a vacuum hot press. The model was used to predict the conditions for thermal buckling of unsupported microchannel fins. Finite element and analytical calculations were found to be in good agreement with experimental results suggesting that thermal buckling of microchannel laminae is possible during the diffusion bonding of microchannel arrays.

Finite element analyses were conducted for different laminae thicknesses and cooling rates to understand the warpage mechanism. It was observed that fin buckling during diffusion bonding was sensitive to the magnitude of the cooling rate and lamina thickness. A relation has been established between the laminae thicknesses and cooling rates. As fin span decreases and fin thickness increases, the allowable cooling rates increase exponentially.

Most MPT devices are presently diffusion bonded at low cooling rates to reduce the effects of thermal stresses. Limits on cooling rates during diffusion bonding of MPT devices investigated in this thesis suggest that with thicker laminae and shorter fin spans, the rate of cooling can be increased leading to significantly reduced cycle times. This would reduce production costs and opens the possibility of applying MPT to more applications.

Implications of the current study are currently limited to copper. However, it is expected that similar findings are likely within a wide variety of microlaminated materials. The present study can be taken as a baseline and should be extended to find cooling rate limitations for the diffusion bonding of MPT devices made from different materials.

REFERENCES

[1] A. A. Abduluyahed and K. J. Kurzydłowski "Tensile Properties of a type 316 stainless steel strained in air and vacuum." Journal of Materials Science and Engineering, Vol. A256, pp. 34-38, 1998

[2] A. A. Rizk, S. F. Radwan, "Fracture of a Plate under Transient Thermal Stresses", Journal of Thermal Stress, v16, pp. 79-102, 1993

[3] A. Y. Tonkovich, S. Fitzgerald, J. L. Zilka, M. J. LaMont, Y. Wang, D. P. Vanderwiel and R. S. Wegeng, " Microchannel Chemical Reactors for Fuel Processing Applications. II. Compact Fuel Vaporization", Proceedings 3rd International conference on Microreaction Technology, 1999, pp. 364-371

[4] B. K. Paul, "Micro energy and chemical systems and multi-scale fabrication", in Micromanufacturing and Nanotechnology, 1st ed., N. P. Mahalik, Ed. Berlin, Germany: Springer-Verlag, pp.323-352, 2006

[5] B. K. Paul and R.B. Peterson "Microlamination for Microtechnology-based Energy, Chemical, and Biological Systems", ASME International Mechanical Engineering Congress and Exposition, Nashville, Tennessee, AES Vol. 39, pp. 45-52, 1999

[6] B. K. Paul, P. Kwon, and R. Subramanian "Understanding limits on fin aspect ratios in counter-flow microchannel arrays produced by diffusion bonding", Journal of Manufacturing Science and Engineering, Vol. 128(4), pp. 977-983

[7] B.K. Paul, S. Bose, D. Palo, An internal convective heating technique for diffusion bonding arrayed microchannel architectures, Precision Engineering, Available online 22 January 2010, ISSN 0141-6359, DOI: 10.1016/j.precisioneng.2010.01.005.

[8] British Stainless Steel Association (BSSA) database, http://www.bssa.org.uk/topics.php?article=139

[9] C. H. Tseng, B. K. Paul, "Sources of Flow Maldistribution in Microreactor-Assisted Synthesis of Ceria Nanoparticles", Ph.D. Dissertation, Oregon State University, 2008

[10] C. Pluess, "Application of Controlled Thermal Expansion in Diffusion Bonding for the High-Volume Microlamination of MECS Devices", M.S. Thesis, Oregon State University, 2004

[11] C. Pluess and B.K. Paul, "Application of controlled Thermal Expansion in Microlamination for the Economical Production of Bulk Microchannel Systems," Chemical Engineering Communications, 194(9), pp. 1259-1270, 2007

[12] D. N. Travessa, M. Ferrante, and G. Ouden "Finite element method simulation of residual stresses in Al_2O_3 – AISI 304 steel joints." Journal of Materials Science and Engineering, Vol. 16, Number 6, pp. 687-691, 2001

[13] D. W. Matson, P. M. Martin, W. D. Bennett, D. C. Stewart and J. W. Johnson, "Laser Machined Microchannel Solvent Separator", Proceedings SPIE, v3223, pp253-259, 1997

[14] D. W. Matson, P.M. Martin, A. Y. Tonkovich and G. L. Roberts, "Fabrication of a Stainless Steel Microcombustor Using a Lamination Process", Proceedings SPIE, v3514, pp386-392, 1998

[15] E. A. Thornton, M. F. Coyle and R. N. McLeod, "Experimental study of plate buckling induced by spatial temperature gradients", Journal of Thermal Stresses, Vol. 17, n 2, pp. 191-210, 1994

[16] G. K. Lingam and B. K. Paul, "Modeling of Microchannel Buckling due to Thermal Stresses during Diffusion Bonding", Thirty-Eighth Annual North American Manufacturing Research Conference (NAMRC), 2010

[17] G. Kovacs, "Micromachined Transducers Sourcebook", McGraw-Hill, New York, 1998

[18] G. Y. Zhou, S. T. Tu, "Viscoelastic analysis of rectangular passage of microchanneled plates subjected to internal pressure," International Journal of Solids and Structures, Vol. 44, n. 21, pp. 6791-6804, 2007

[19] H. Loewe and W. Ehrfeld "State-of-the-Art in Microreaction Technology: Concepts, Manufacturing and Applications", Electrochimica Acta, Vol. 44, pp. 3679-3689, 1998

[20] J. Feng, D.Wang, H. Liu and Z. Li "Finite element simulation of thermal stresses during diffusion bonding of Al2O3 ceramic to Aluminum." Science and Technology of Welding and Joining, Vol. 8, Number 2, pp. 138-142, 2003

[21] J. R. Davis, Metals Handbook, Materials Park, Ohio: ASM International, 1998

[22] J. X. Zhang, R.S. Chandel, Y.Z. Chen, and H.P. Seow "Effect of residual stress on the strength of an alumina-steel joint by partial transient liquid phase (PTLP) brazing." Journal of Materials Processing Technology, pp. 220-225, 2000

[23] K. Schubert, J. Brandner, M. Fichtner, G. Linder, U. Schygulla and A. Wenka, "Microstructure devices for applications in thermal and chemical process engineering," Microscale Thermophysical Engineering, v 5, n 1, pp. 17-39, 2001

[24] M. Koch, A. Evans, and A. Brunnschweiler, "Microfluidic Technology and Applications", Research Studies Press Ltd., Hertfordshire, England, 2000

[25] M. L. Gossard, P. Seide, W. M. Roberts, "Thermal buckling of plates," NACA Technical Note 2771, Document ID# 19930083554, pp. 1-40, 1952

[26] N. A. Alfutov, translated by E. Evseev, V. B. Balmont, Stability of Elastic Structures, Berlin; New York: Springer, 2000

[27] P. M. Martin, D. W. Matson, W. D. Bennett, D. C. Steward, Y. Lin, Laser Micromachined and Laminated Microfluidic Components for Miniaturized Thermal, Chemical and Biological Systems", Proceedings of SPIE, v. 3680, p. 826-833, 1999

[28] P. M. Martin, W. D. Bennett and J. W. Johnson, "Microchannel Heat Exchangers for Advanced Climate Control", Proceedings, SPIE, v2639, pp82-88, 1996

[29] R. L. Templin et al., Properties of Metals in Materials Engineering, Cleveland, 1948

[30] R. M. Jones, “Plastic Thermal Buckling of Uniformly Heated Plates with Temperature-Dependent Material Properties, AIAA 2004-1709

[31] R. M. Jones, “Plastic Thermal Buckling of Uniformly Heated Bars with Temperature-Dependent Material Properties, AIAA 2005-1935

[32] S. Bose, B. K. Paul, “An Internal Convective Heating Technique for Diffusion Bonding Highly Parallel Microchannel Architectures”, M.S. Thesis, Oregon State University, 2008

[33] S. Bose, D. R. Palo and B. K. Paul “Leakage Rates in Thermal Requirements for the Diffusion Bonding of Microchannel Arrays via Internal Convective Heating”, 2nd International Conference on Micromanufacturing, 2007

[34] S. K. Tiwari and B.K. Paul “Application of Nickel Nanoparticles in Diffusion Bonding of Stainless Steel Surfaces”, ASME International Conference on Manufacturing Science and Engineering (MSEC), 2008

[35] T. R. Tauchert, “Thermally induced flexure, buckling, and vibration of plates”, Applied Mechanics Reviews, Vol. 44, n 8, pp. 347, 1991

[36] U. S. Patent No. 5,611,214, “Microcomponent sheet architecture” R. S. Wegeng, K. M. Drost, C. E. McDonald, 1997

[37] U. S. Patent No. 5,811,062, “Microchannel chemical process sheet architecture” R. S. Wegeng, K. M. Drost, C. J. Call, J. G. Brimingham, C. E. McDonald, D. E. Kurath, M. Fredrich, 1998

[38] W. Ehrfeld, V. Hessel, H. Lowe, Chapter 2, “Modern Microfabrication Techniques for Microreactors”, New Technology for Modern Chemistry, Wiley-VCH, New York, pp. 30-33, 2000

[39] W. Fang and J. A. Wickert, “Post buckling of micromachined beams”, Journal of Micromechanics and Microengineering, Vol. 4, pp. 116-122, 1994

[40] W. Wattanutchariya and B.K. Paul "Bonding fixture tolerances for high-volume metal microlamination based on fin buckling and laminae misalignment behavior." Journal of Precision Engineering, Vol. 28, pp. 117-128, 2004

APPENDIX A

Test Article Design and Features Sizes

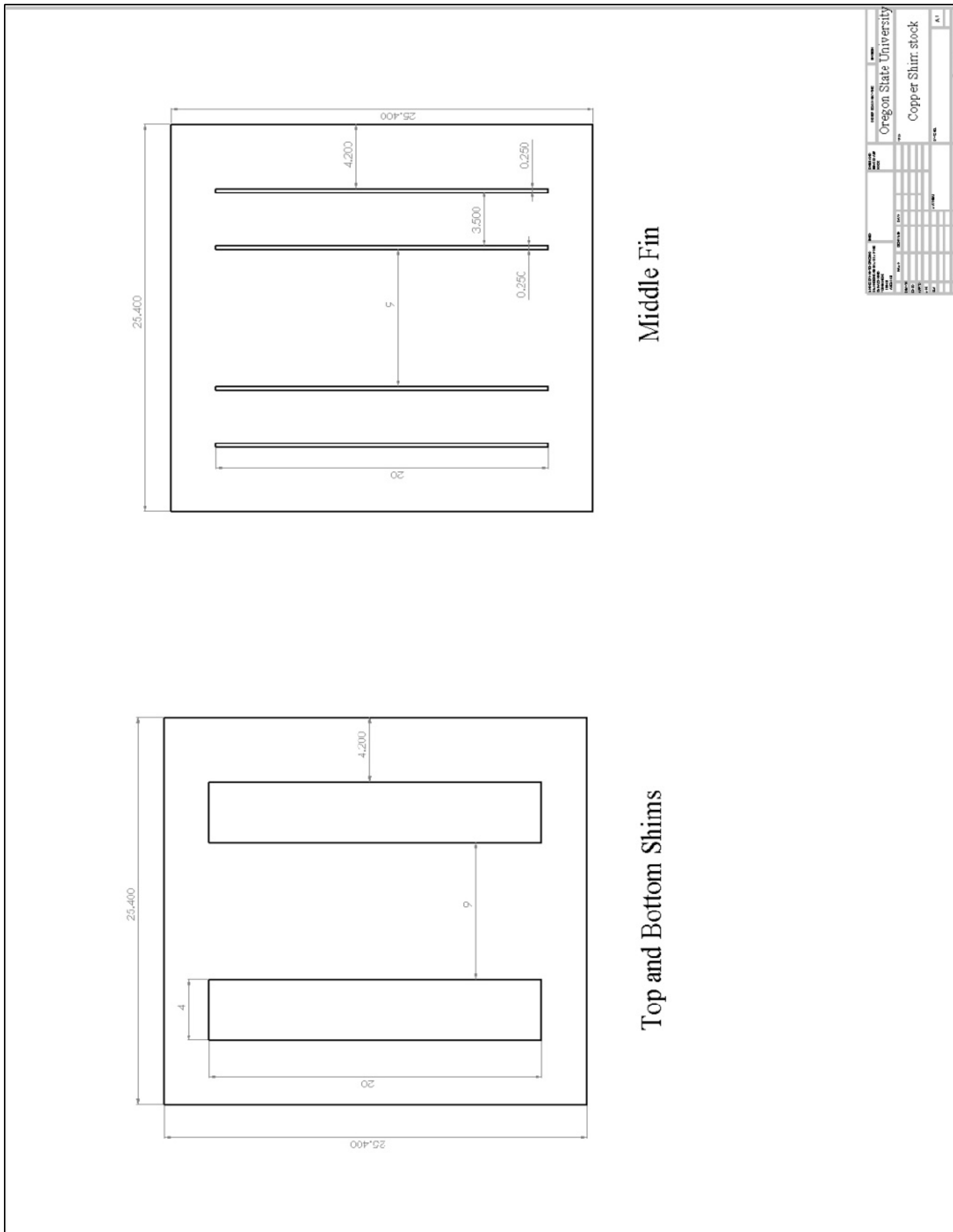

Test Article Assembly with Ceramic Platens

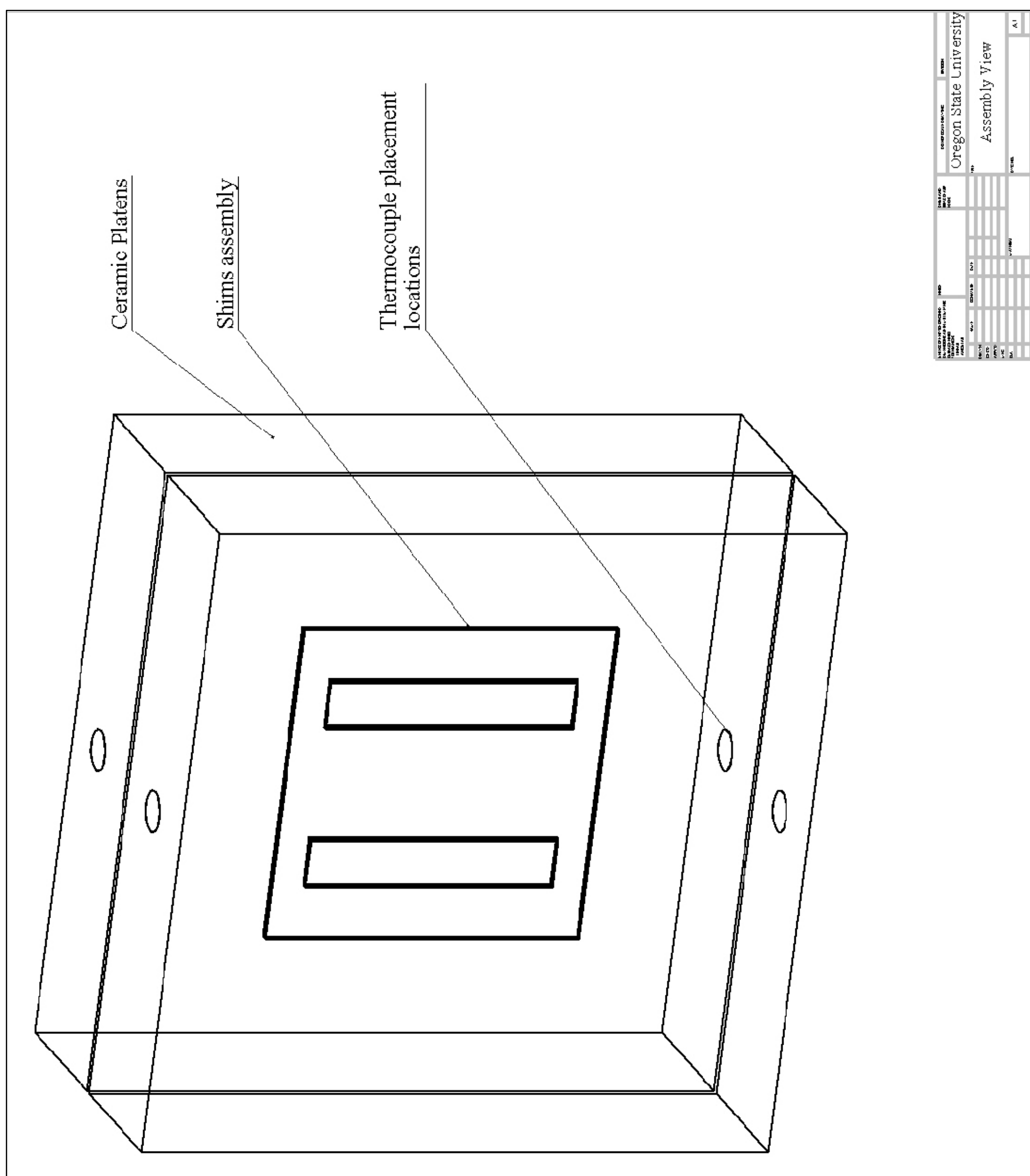

Combinations of Experimental Runs made

Channel laminae thickness (µm)	**Fin lamina thickness (µm)**	**Cooling rate (°C/min)**
200	50	2
	50	3.5
	50	14
200	75	2
	75	11
	75	14
200	100	3.5
	100	5
	100	10
200	200	8
	200	11
	200	14

APPENDIX B

FE-Model Settings for Analyses

```
**
** MATERIALS
**
*Material, name=Copper
*Conductivity
401., 273.
398., 300.
357.,1073.
*Density
8930., 293.
7940.,1073.
*Elastic
 1.14e+11, 0.343,  297.
  1.1e+11,  0.34,  373.
  9.8e+10,  0.32,  477.
  5.5e+10,   0.3,  727.
  2.5e+10,  0.28, 1073.
*Expansion
 1.64e-05, 293.
 1.85e-05,1023.
*Plastic
 3.39e+07,   0.
1e+11, 0.15
```

```
*Specific Heat
385.,
**
** PHYSICAL CONSTANTS
**
*Physical Constants, absolute zero=-273., stefan boltzmann=5.68e-08
**
** PREDEFINED FIELDS
**
** Name: Predefined Field-1   Type: Temperature
*Initial Conditions, type=TEMPERATURE
_PickedSet9, 1073.
** ----------------------------------------------------------------
**
** STEP: Step-1
**
*Step, name=Step-1, extrapolation=PARABOLIC, inc=200
*Static
0.01, 300., 0.003, 20.
**
** BOUNDARY CONDITIONS
**
** Name: BC-1 Type: Displacement/Rotation
*Boundary
_PickedSet8, 3, 3
**
```

** PREDEFINED FIELDS

**

** Name: Predefined Field-2   Type: Temperature

*Temperature, file=D:/Temp/200X200X200-14Cmin.odb, bstep=1, binc=1, estep=1, einc=19, midside

**

** OUTPUT REQUESTS

**

*Restart, write, frequency=0

**

** FIELD OUTPUT: F-Output-1

**

*Output, field, variable=PRESELECT

**

** HISTORY OUTPUT: H-Output-1

**

*Output, history, variable=PRESELECT

*End Step

APPENDIX C

Properties of Stainless Steel at Higher Temperatures

Temperature (K)	Young's Modulus (GPa)	Conductivity (W/m-K)	Specific heat (J/Kg-k)	Yield Stress (MPa)	Co-efficient of thermal expansion (μm/m-K)	Poisson's ratio
300	194.18	13.40	468	206.85	15.156	0.28
400	188.49	15.20	504	167.49	16.051	0.28
500	182.02	16.75	527	143.38	16.933	0.30
600	174.29	19.30	550	128.64	17.511	0.32
700	166.17	19.80	563	121.36	17.946	0.28
800	157.96	21.30	576	117.62	18.297	0.29
900	148.63	22.75	589	112.52	18.592	0.28
1000	136.50	24.20	602	102.99	18.847	0.25

Mechanical and Thermal Properties of Copper at Higher Temperatures

Temperature (K)	Young's Modulus (GPa)	Poisson's ratio	Conductivity (W/m-K)	Co-efficient of thermal expansion (μm/m-K)
297	114	0.343	401	16.4
373	110	0.34	398	
477	98	0.3		
727	55	0.3		
1073	25	0.28	357	18.5

APPENDIX D

FE-Model Results

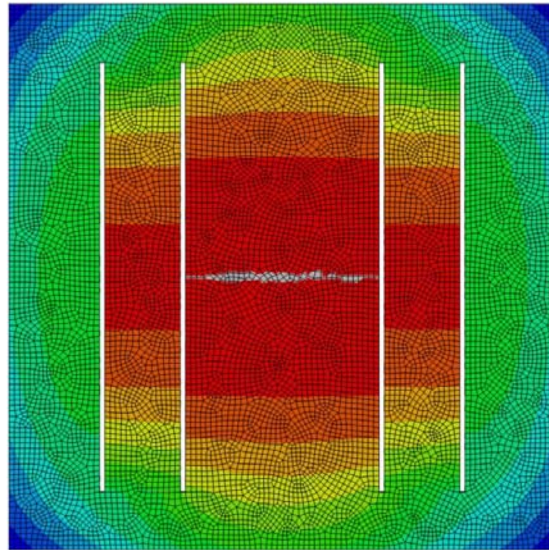

(a)

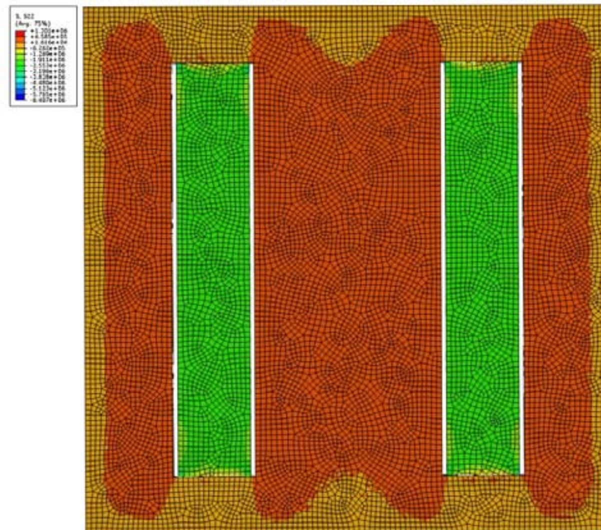

(b)

Figure E-1. *(a) Temperature distribution and (b) stress distribution in 50μm shim, run at a cooling rate of 2℃/min*

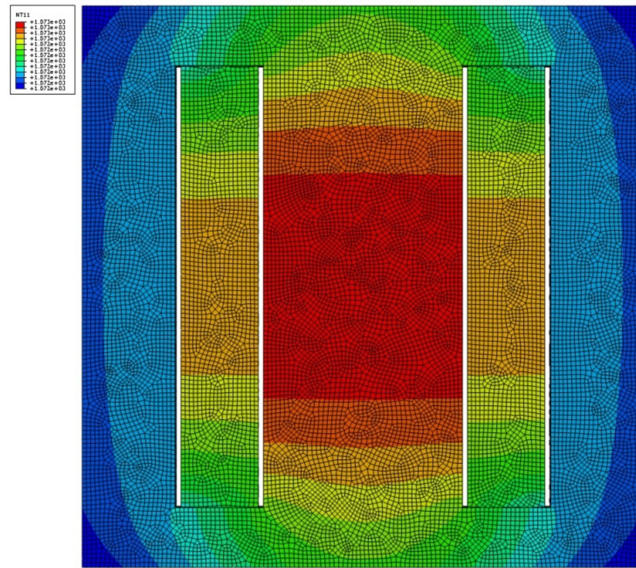

(a)

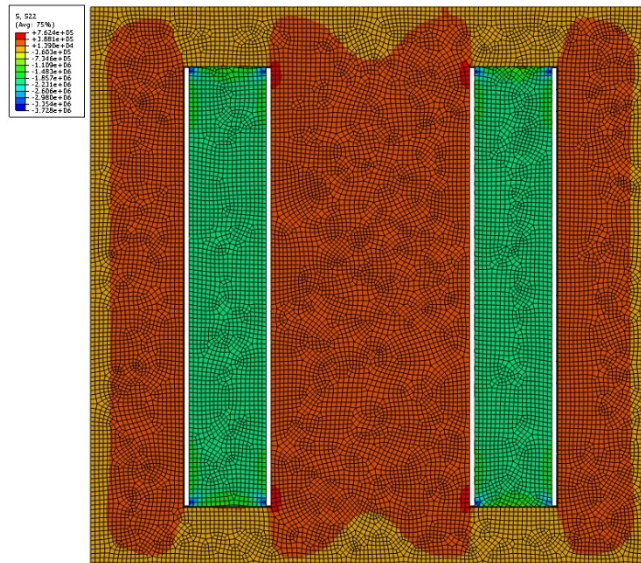

(b)

Figure E-2. *(a) Temperature distribution and (b) stress distribution in 75μm shim, run at a cooling rate of 2℃/min*

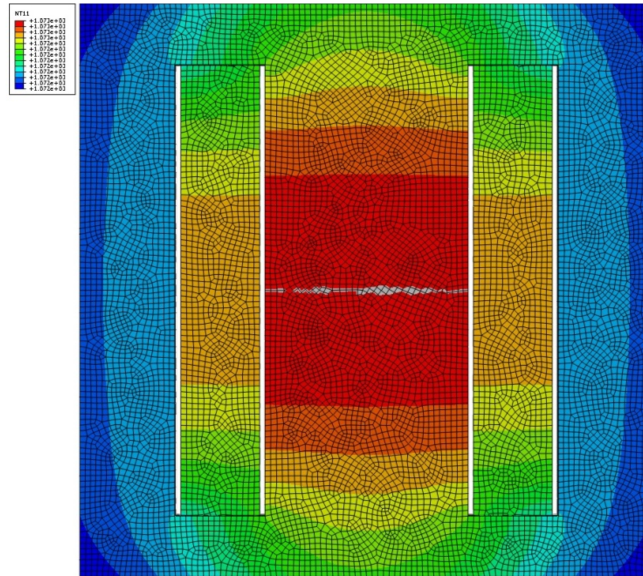

(a)

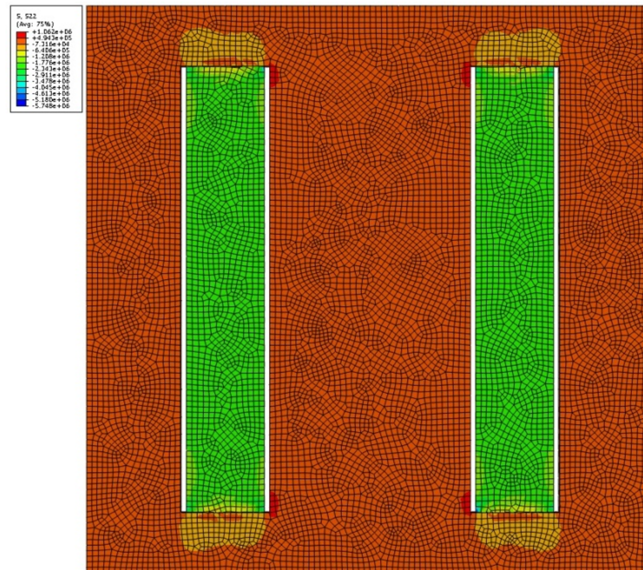

(b)

Figure E-3. *(a) Temperature distribution and (b) stress distribution in 100μm shim, run at a cooling rate of 3.5℃/min*

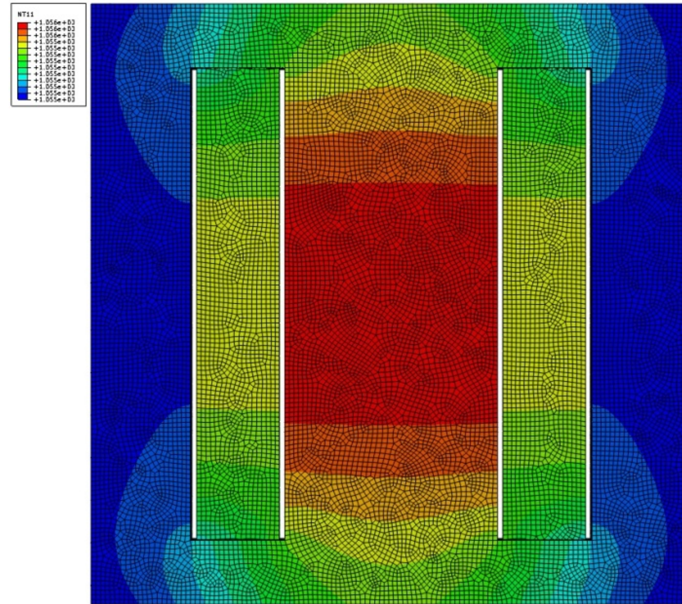

(a)

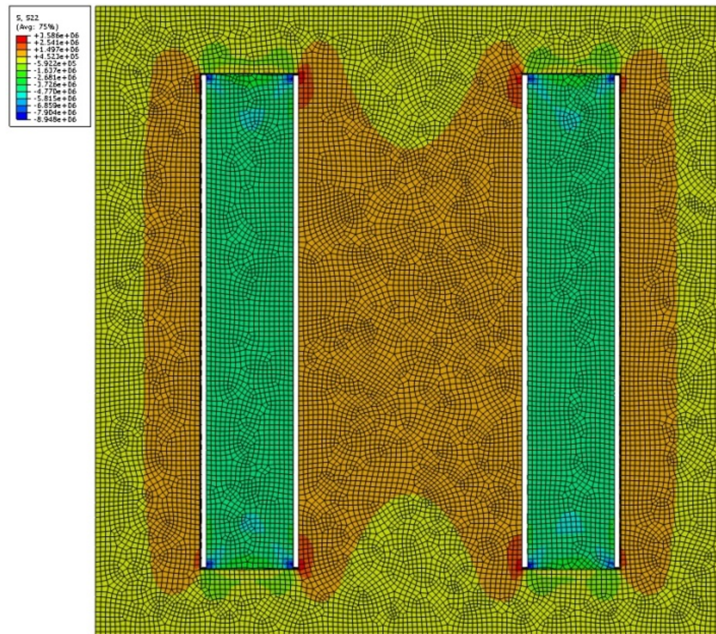

(b)

Figure E-4. *(a) Temperature distribution and (b) stress distribution in 200µm shim, run at a cooling rate of 8℃/min*

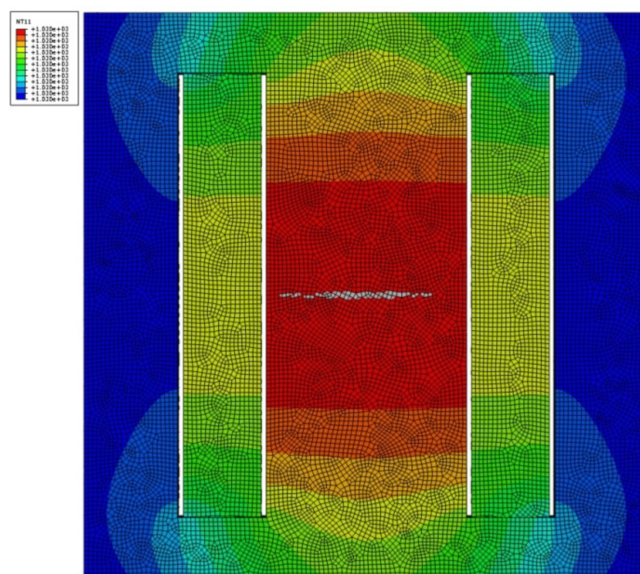

(a)

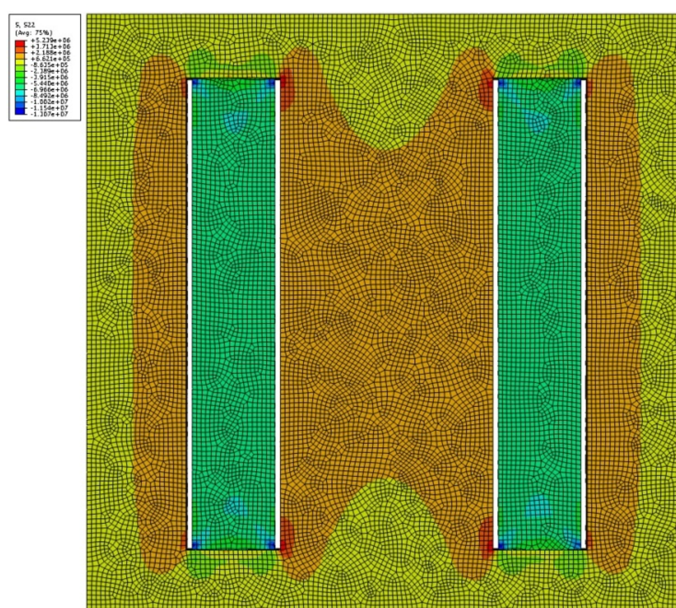

(b)

Figure E-5. *(a) Temperature distribution and (b) stress distribution in 200µm shim, run at a cooling rate of 11°C/min*

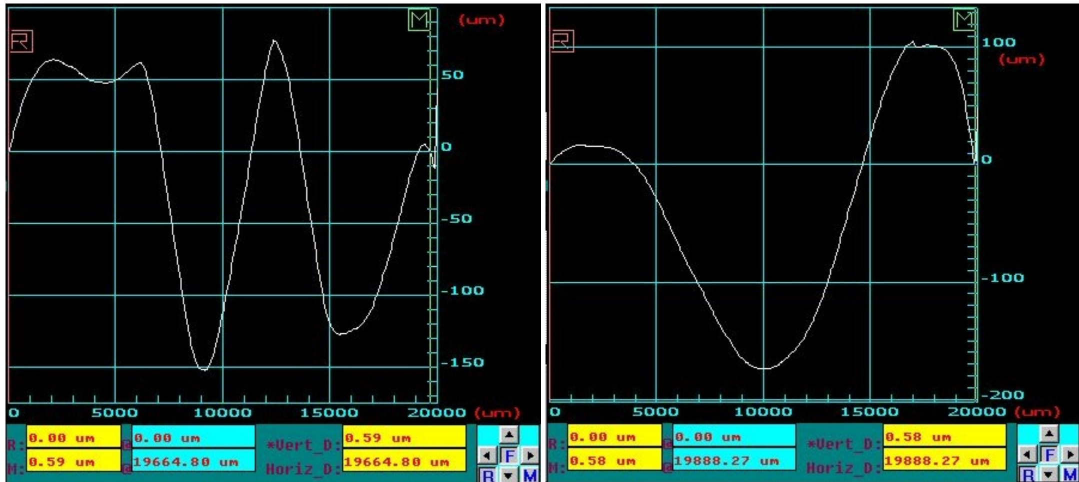

(a) (b)

Figure E-6.*Profiler scans of 50µm thick fins bonded at a cooling rate of 2ºC/min*

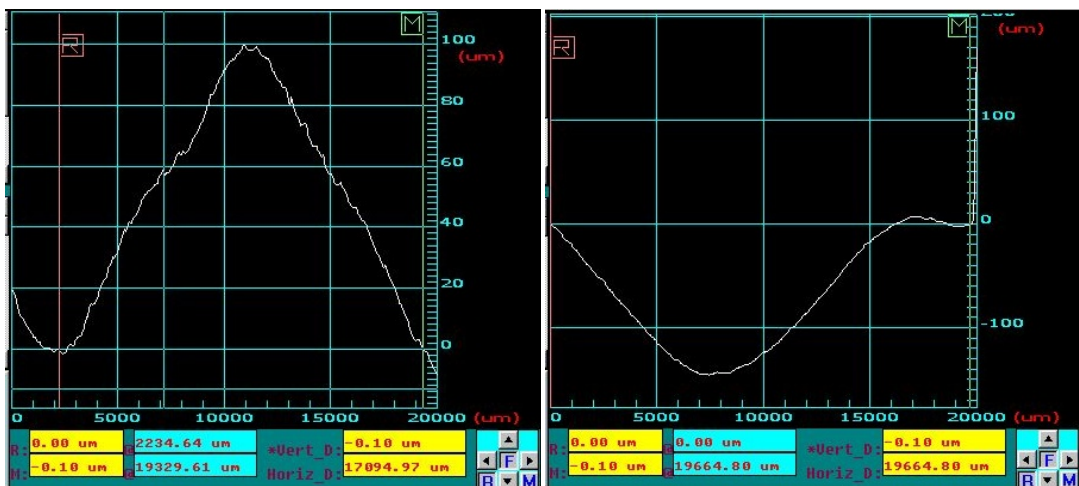

(a) (b)

Figure E-7.*Profiler scans of fins of thickness 75µm bonded at a cooling rate of (a) 2ºC/min and (b) 3.5ºC/min*

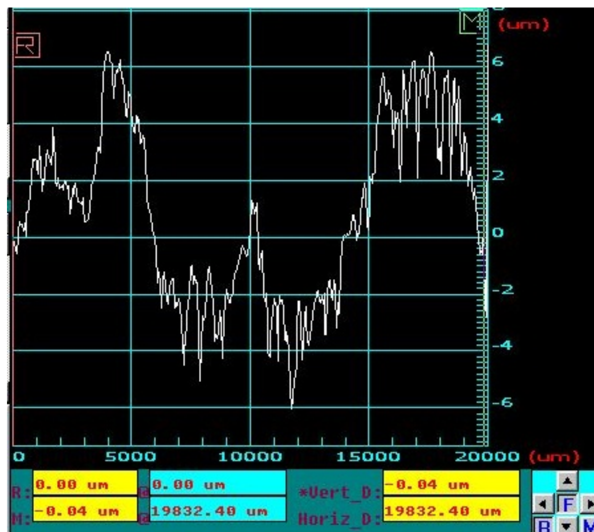

Figure E-8.*Profiler scan over a length of 15mm on the fin of thickness 200µm cooled at a rate of 8°C/min*

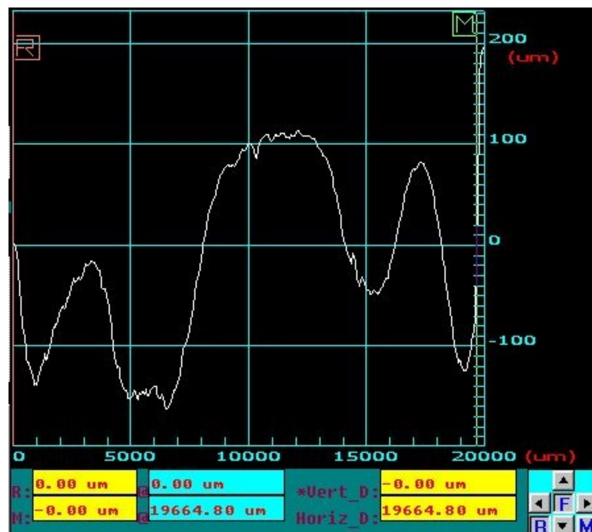

Figure E-9.*Profiler scan over a length of 15mm on the fin of thickness 200µm cooled at a rate of 11°C/min*